THESIS APPROVAL

GRADUATE SCHOOL, KASETSART UNIVERSITY

Master of Science (Chemistry)
DEGREE

Chemistry   Chemistry
FIELD   **DEPARTMENT**

TITLE: 4-Ethynyl-*N,N*-Dimethylaniline and 1-Ethynyl-4-Methylbenzene Derivatives with Bromoarene Nucleus for Oleds Devices : Sonogashira Coupling, Microwave-Assisted Synthesis, Spectral Properties and Theoretical Studies

NAME: Miss Panida Maneekobkulwong

THIS THESIS HAS BEEN ACCEPTED BY

_____ **THESIS ADVISOR**
(_____ Mr. Songwut Suramitr, Ph.D. _____)

_____ **THESIS CO-ADVISOR**
(_____ Mr. Surachai Thachepan, Ph.D. _____)

_____ **DEPARTMENT HEAD**
(_____ Associate Professor Supa Hannongbua, Dr.rer.nat. _____)

APPROVED BY THE GRADUATE SCHOOL ON _____

_____ **DEAN**
(_____ Associate Professor Gunjana Theeragool, D.Agr. _____)

THESIS

4-ETHYNYL-*N,N*-DIMETHYLANILINE AND 1-ETHYNYL-4-
METHYLBENZENE DERIVATIVES WITH BROMOARENE
NUCLEUS FOR OLEDS DEVICES: SONOGASHIRA COUPLING,
MICROWAVE-ASSISTED SYNTHESIS, SPECTRAL PROPERTIES
AND THEORETICAL STUDIES

PANIDA MANEEKOBKULWONG

A Thesis Submitted in Partial Fulfillment of

the Requirements for the Degree of

Master of Science (Chemistry)

Graduate School, Kasetsart University

2012

Panida Maneekobkulwong 2012: 4-Ethynyl-*N,N*-Dimethylaniline and 1-Ethynyl-4-Methylbenzene Derivatives with Bromoarene Nucleus for Oleds Devices : Sonogashira Coupling, Microwave-Assisted Synthesis, Spectral Properties and Theoretical Studies. Master of Science (Chemistry), Major Field: Chemistry, Department of Chemistry. Thesis Advisor: Mr. Songwut Suramitr, Ph.D. 76 pages.

4-Ethynyl-*N,N*-dimethylaniline and 1-ethynyl-4-methylbenzene derivatives of aryl-pi-donor molecules has been synthesized and studied with respect to their photophysical properties. Microwave-assisted, palladium-catalyzed Sonogashira-type couplings of terminal acetylenes with 4-bromobipheny, 2-bromofluorene and l-bromopyrene are the latest strategies in this endeavour. All molecules show absorption in the near-visible region and emission in the visible region. Bright solid-state photoluminescence has also been noticed for all the compounds in the visible region. The density functional theories (DFT) were investigated for support the experimental observations. A fast, simple and effective procedure for the synthesis of aryl-pi-donor dyes under microwave irradiation condition can been used for novel tunable organic materials.

_____   _____   ___ / ___ / ___

Student's signature   Thesis Advisor's signature

ACKNOWLEDGEMENTS

Panida Maneekobkulwong

November 2012

TABLE OF CONTENTS

Page

LIST OF TABLES

LIST OF FIGURES

LIST OF FIGURES (Continued)

LIST OF FIGURES (Continued)

LIST OF FIGURES (Continued)

LIST OF ABBREVIATIONS

OLEDs	=	Organic light emitting diodes
UV-Vis	=	Ultraviolet-visible spectroscopy
^{1}H NMR	=	Proton Nuclear Magnetic Resonance
FT-IR	=	Fourier Transform Infrared Spectroscopy
A	=	1-ethynyl-4-methylbenzene
1**A**	=	4-(biphenyl-4-ylethynyl)-methylbenzene
2**A**	=	4-((4aH-fluoren-7-yl)ethynyl)- methylbenzene
3**A**	=	4-(pyren-1-ylethynyl)- methylbenzene
B	=	4-ethynyl-*n,n*-dimethylaniline
1**B**	=	4-(biphenyl-4-ylethynyl)-*N,N*-dimethylaniline
2**B**	=	4-((4aH-fluoren-7-yl)ethynyl)-*N,N*-dimethyl aniline
3**B**	=	4-(pyren-1-ylethynyl)-*N,N*-dimethylaniline
Hex	=	hexane
EtOAc	=	ethyl acetate
DCM	=	dichloromethane
EtOH	=	ethyl alcohol
ACN	=	Acetonitrile
DMSO	=	Dimethyl sulfoxide
THF	=	tetrahydrofuran
MW	=	Microwave
DFT	=	density functional theory
TDDFT	=	time-depend density functional theory
PCM	=	polarizable continuum model
LR	=	linear response
SS	=	state-specific
TLC	=	Thin Layer Chromatography
HOMO	=	Highest Occupied Molecular Orbital
LUMO	=	Lowest Unoccupied Molecular Orbital

4-ETHYNYL-*N,N*-DIMETHYLANILINE AND 1-ETHYNYL-4-METHYLBENZENE DERIVATIVES WITH BROMOARENE NUCLEUS FOR OLEDS DEVICES : SONOGASHIRA COUPLING, MICROWAVE-ASSISTED SYNTHESIS, SPECTRAL PROPERTIES AND THEORETICAL STUDIES

INTRODUCTION

Organic light emitting diodes (OLEDs) technology are devices that can be used for small screen mobile displays, lighting and TVs. Industry giants such as Sony, LG and Kodak amongst others are developing screens that are just millimetres thick and have a far sharper picture than plasma or LCD screens. Unlike existing screens which need a backlight, OLED pixels radiate light, making them far more energy efficient (Borrett, 2010). A typical OLED consists of two organic layers (electron and hole transport layers), embedded between two electrodes (in Figure 1).
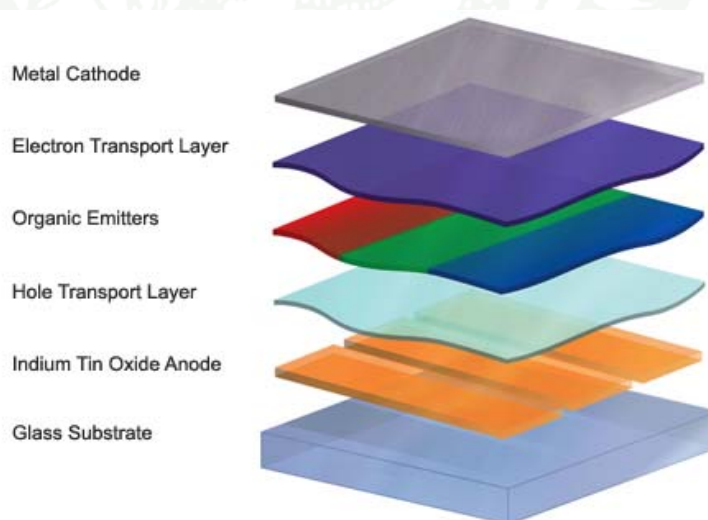
Figure 1 Construction of an OLED Organic Light Emitting Diode Diagram.

Source: Fleischmann (2007)

The top electrode is usually a metallic mirror with high reflectivity and the bottom electrode a transparent ITO layer on top of the glass substrat. OLEDs are electronic devices made by placing a thin film of an electroluminescent organic material between two conductors of different work functions. When an electrical voltage is applied, electrons and holes are injected into the electroluminescent material. When these recombine, light is emitted. Additional thin film layers are usually added for different purposes such as electron and hole transport (Morgado *et al.*, 2003). Different materials and dopants can be used to generate different colors.

In Figure 2, when a voltage is applied to the electrodes the charges start moving in the device under the influence of the electric field. Electrons leave the cathode and holes move from the anode in opposite direction. The recombination of this charges leads to the creation of a photon with a frequency given by the energy gap ($E = hv$) between the LUMO and HOMO levels of the emitting molecules (Angel, 2008).
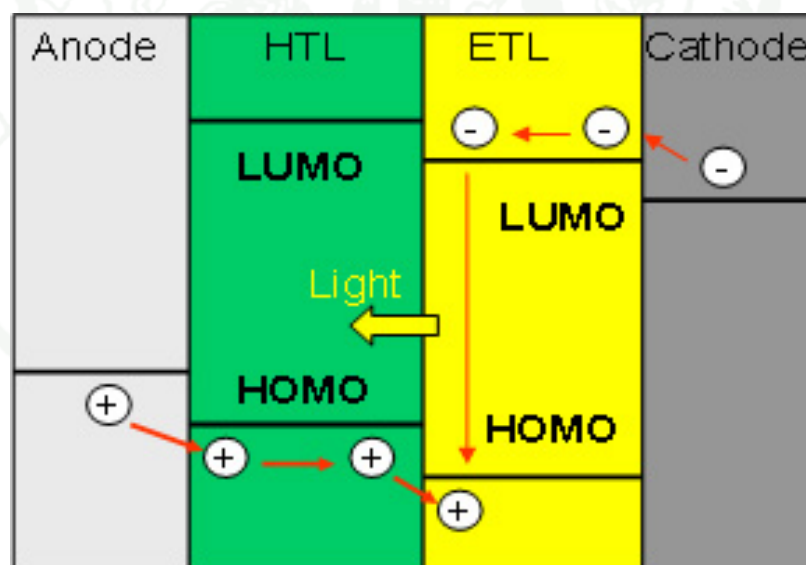
Figure 2 Charge transport and light generation in OLED's.

Source: (Angel, 2008)

During last decade, the intensive research has been carried out to generate the material with high light emitting efficiencies, high thermal stability, and good amorphous film formation property (Gigante *et al.*, 2009). The electro-luminescence (EL) characteristic of OLEDs materials depend on the appropriate HOMO and LUMO energy levels and the electron and hole motilies (Brunner *et al.*, 2004; Holmes *et al.*, 2003). The examples OLED materials are shown in Figure 3.
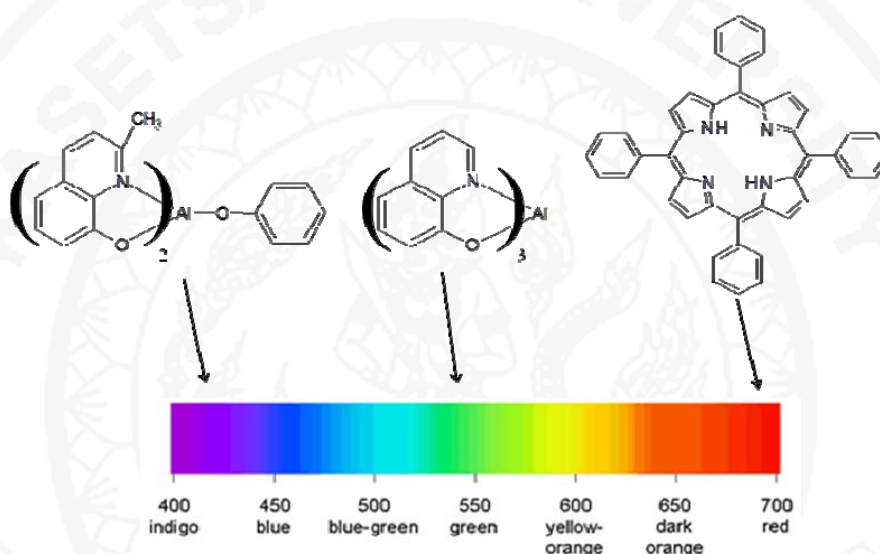
Figure 3 light emitting molecules.

With regard to device fabrication, organic light emitting diodes can be classified into two general families: those that can be processed into devices by vacuum deposition (small molecules) or by solution processing (polymers). Small molecules are advantageous because they can be purified by common techniques such as recrystallization, chromatography, and sublimation and vacuum deposited in multilayer stacks, both important for device lifetime and efficiency However, vacuum-deposition techniques require costly processes that are limited to practical substrate size and relatively low yields in the manufacture of high volume products using masking technologies.

Architecture of π-conjugated aromatic compounds assumes significance in view of the application of these compounds in nonlinear optics (NLO), in organic light-emitting diodes (OLEDs), in polymer LEDs, in carbohydrate sensors, in electro generated chemiluminescence (ECL), as photoconductors, and in molecular electronics and other optoelectronic applications. Design and synthesis of compounds by Sonogashira cross-coupling of terminal acetylenes with bromoarenes are the latest strategies in this endeavor. Coupling of donor-arylethynyl moieties with common acceptor aromatic fluorophores would enable us to achieve new molecules. Such compounds are called organic mixed valence compounds and are useful probes for adiabatic electron transfer processes, and their novel properties would make them suitable candidates for the said application. A polycyclic aromatic compound such as biphenyl is well-known emitters and their photophysical properties have been well-established and well-exploited for various applications (Ho *et al.*, 2005).

The Sonogashira reaction, a Pd-catalyzed cross-coupling between aryl halides and terminal alkynes, is a powerful tool for the synthesis of various aryl alkynes, although the use of copper salts, toxic phosphine ligands, amines and homogenous Pd catalysts are generally difficult to recover and reuse. Recently, several procedures were published describing the application of this coupling to the less reactive aryl bromides and triflates involving long reaction times (Brase *et al.*, 2002).

Attempts to improve this reaction would have to address some of its weaknesses: the demand for a reactive arene derivative, long reaction times, and the limited choice of reaction medium. Microwave heating has emerged as a versatile method to speed up many chemical reactions, delivering high yields in a few minutes, and has consequently been applied to the Sonogashira reaction. When microwave heating was first used in a heterogeneous phase system, several hours or even days were required for full conversion.

Microwave (MW) irradiation is widely used to promote chemical reactions and a number of reviews have advocated the use of MW technology in organic synthesis. Microwave activation as a non-conventional energy source is becoming a

very popular and useful technique in organic chemistry. The combination of solvent-free reaction conditions and microwave irradiation leads to significantly reduced reaction times, enhanced conversions and sometimes higher selectivity with several advantages for the eco-friendly approach, termed green chemistry. Recently, a fast, solventless, microwave-assisted heterogeneous Sonogashira coupling on alumina has been achieved, but the reaction was limited to aryl iodides. To date, a microwave-assisted Sonogashira reaction in the homogeneous phase has not been reported. In fact, it has been recommended to avoid homogeneous conditions, because of the difficulty of controlling the reaction rate in the presence of volatile liquid reactants and metal catalyst that can cause thermal runaway (Changdev *et al.*, 2009).

In the present work, we attempt to modify the synthesis procedures, Sonogashira reaction in the homogeneous phase, to synthesize *N,N*-dimethylaniline and methylbenzene-functionalized with ethynyl arene derivative under microwave irradiation conditions. The photophysical properties were then studied of the synthesized compounds and compared them with a standard compound of similar kind, which is already reported in the literature. Finally, the structural and electronic properties were explained by using density functional theory (DFT) based theoretical calculations.
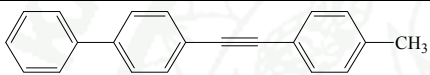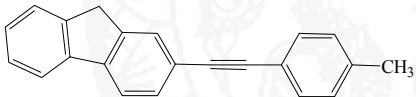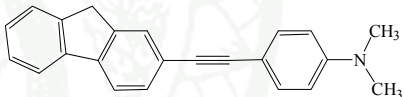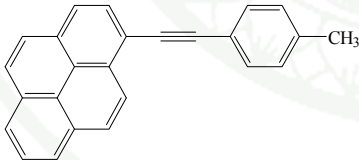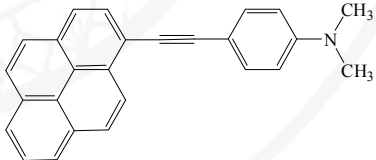
OBJECTIVES

There are three main objectives that this work focuses on;

1. To synthesize and characterize of 1-ethynyl-4-methylbenzene and 4-Ethynyl-*N*,*N*-dimethylaniline derivatives show in Table 1.

Table 1 Structures of compound to synthesize.

1-ethynyl-4-methylbenzene (**A**)	4-Ethynyl-*N*,*N*-dimethylaniline (**B**)
4-(biphenyl-4-ylethynyl)-methylbenzene (1**A**)	4-(biphenyl-4-ylethynyl)-*N*,*N*-dimethylaniline (1**B**)
4-((4aH-fluoren-7-yl)ethynyl)-methylbenzene (2**A**)	4-((4aH-fluoren-7-yl)ethynyl)-*N*,*N*-dimethylaniline (2**B**)
4-(pyren-1-ylethynyl)-methylbenzene (3**A**)	4-(pyren-1-ylethynyl)-*N*,*N*-dimethylaniline (3**B**)

2. To studies the photophysical properties of 1-ethynyl-4-methylbenzene and 4-Ethynyl-*N*,*N*-dimethylaniline derivatives.

3. To investigate the structural and electronic properties of 1-ethynyl-4-methylbenzene and 4-Ethynyl-*N*,*N*-dimethylaniline derivatives by using density functional theory (DFT).

LITERATURE REVIEW

Since the first discovery of organic light-emitting devices (OLEDs) by Tang and co-workers, materials and devices of OLEDs have drawn much attention due to their potential application in flat panel display (Liao *et al.*, 2004). Recently, organic light-emitting diodes based on guest/host emitters were found to give extremely excellent high luminance as well as current and power efficiency (Lee *et al.*, 2004). OLEDs using anthracene derivatives as guest/host emitters have been reported to exhibit very excellent performance and have potential for fluorescent materials (Park *et al.*, 2010). A variety of bulky functional groups have been designed to prevent the intermolecular stacking of anthrancene to increase fluorescent quantum yield, device lifetime and color purity (Pu *et al.*, 2010).

The optical designs of planar and non-planar OLEDs were developed. An OLED consists of a stacked thin film, with effective optical length comparable to the visible wavelength. Hence, EL from such a device experiences an interference effect and can be viewed as a Fabry-Perot cavity. By engineering the organic layer thicknesses, together with different anode and cathode structures, it is possible to optimize the optical intensity and select desired emission wavelength. However, there is unavoidable wave guiding light in the organic, ITO, and glass substrate. Non-planar structures can effectively extract out those photons to boost the efficiency. By introducing a corrugated structure at the device side, the organic and SPR mode can be effectively extracted. On the other hand, thin films with microstructures attached on the glass substrate can reduce the TIR and extract out the glass substrate mode (Wei *et al.*, 2010).

The quest for new and improved organic semiconductors continues with emphasis on optimizing key properties such as luminescence, absorption, energy band gaps, charge transport, and stability (Shirota and Kageyama, 2007). With regard to device fabrication, organic semiconductors can be classified into two general families: those that can be processed into devices by vacuum deposition (small molecules) or by solution processing (polymers). Small molecules are advantageous because they

can be purified by common techniques such as recrystallization, chromatography, and sublimation and vacuum deposited in multilayer stacks, both important for device lifetime and efficiency. However, vacuum-deposition techniques require costly processes that are limited to practical substrate size and relatively low yields in the manufacture of high volume products using masking technologies (Shtein *et al.*, 2004). (Sonar *et al.*, 2010) interest lies in materials that combine the advantages of both small molecules and polymers, specifically monodisperse star-shaped materials with high purity and solution process.

Ho *et al.* (2005) were synthesized aryl-π-donor-aryl molecules has been synthesized and studied with respect to their photophysical properties and electrogenerated chemiluminscence (ECL) for the first time. Anthracene, phenanthrene, naphthalene, biphenyl, and fluorene were coupled with *N,N*-dimethylanilino moiety via a C-C triple bond (1-7). Introduction of such a strong electron-donating moiety as *N,N*-dimethylanilino group through a triple bond imparts new properties to the resultant molecules that are not commonly observed for the parent arenes. All molecules show absorption in the near-visible region and emission totally in the visible region with high fluorescence quantum yields. Bright solid-state photoluminescence has also been noticed for all the compounds in the visible region.
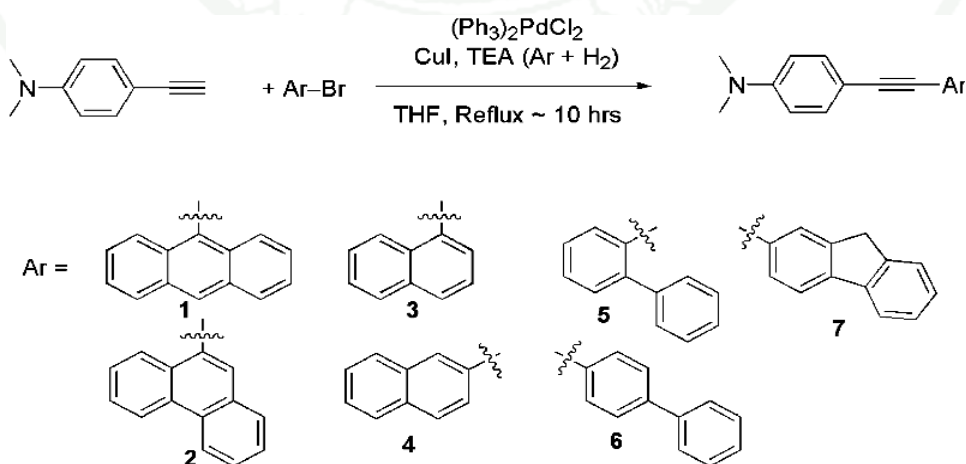
Figure 4 Synthesis of the Fluorophores 1-7 by Coupling of Bromoarenes with p-*N,N*-Dimethylanilinoalkyne.

They have tailor-made new and simple ethyne-based highly fluorescence emitting molecules and studied their ECL and other photophysical properties. Though the electrochemical characteristics do not show many variations among 1-7, the ECL behavior is quite different. Compounds 1 and 3 show blue-shifted ECL emission compared to their photoluminescence. Compound 5 shows monomeric ICT ECL and 6 shows excimer ECL emission. Although there is no ECL activity for 2, 4, and 7, the excellent fluorescence properties in solutions and in solid films of these and all the compounds in general would be useful for application as probes in analytical studies and in optoelectronic devices. The methyl substuents on the N-diarryl rings of anthracene- 9,10-diamine showed obvious effects in emission spectra as demonstrated in photo-studies, which observedma significant bathochromic shift The effect of methyl groups substituted at both the para/meta positions of the N-diarryl rings of anthracene-9,10-diamine could show great improvement in device performance as compared to the non-substituent compound TAD (Yu *et al.*, 2011).

Yang *et al.* (2004) were synthesized via Sonogashira coupling reactions of 2-bromo-, 2,6-dibromo-, and 2,7-dibromo-9,10-anthraquinone with para-substituted phenylacetylenes. While the redox properties of those compounds are almost insensitive to substitution, their absorption maxima are linearly related to the Hammett constants with different slopes for electron donors and electron acceptors. The charge-transfer character of the emitting state is supported by large dipole moment differences between the ground and the excited state as concluded on the basis of molecular modeling and Lippert-Mataga correlations of the Stokes shifts with solvent polarity. Maximum Stokes shifts are attained by both electrondonating and withdrawing groups. This is explained by a destabilization of the HOMO by electron donors and a stabilization of the LUMO by electron acceptors (Kapoor and Thomas, 2010).

Microwave (MW) irradiation is widely used to promote chemical reactions and a number of reviews have advocated the use of MW technology in organic synthesis. Microwave activation as a non-conventional energy source is becoming a very popular and useful technique in organic chemistry. The combination of solvent-

free reaction conditions and microwave irradiation leads to significantly reduced reaction times, enhanced conversions and sometimes higher selectivity with several advantages for the eco-friendly approach, termed green chemistry (Larhed and Hallberg, 1996).

Recently a fast and solvent less microwave-assisted heterogeneous and homogeneous Sonogashira coupling has been reported on aryl halides and acetylene moieties (Erdélyi and Gogoll, 2001). But not reported on benzimidazole compounds. Conventional syntheses of aryl benzimidazoles were reported and Sonogashira coupling were done by standard procedure. Previously, the microwave-assisted syntheses of benzimidazoles were reported on aryl acid with *o*-phenylenediamine.
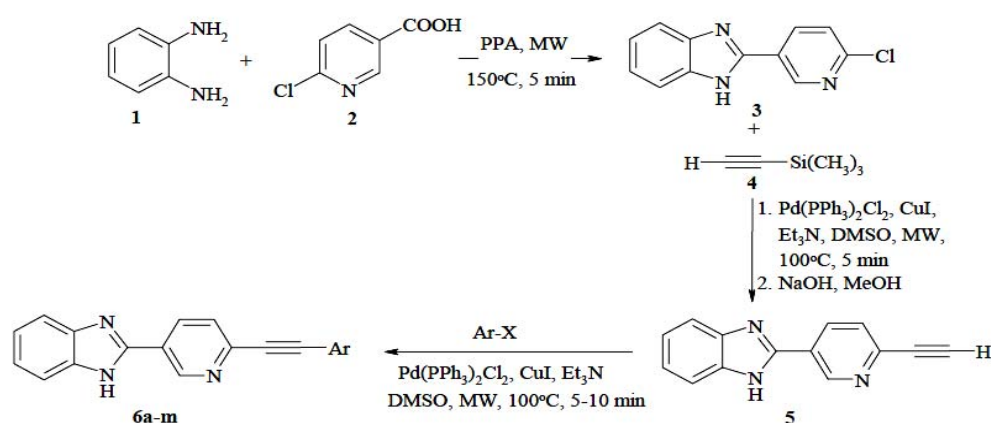
Figure 5 Sonogashira coupling microwave-assisted syntheses of benzimidazoles.

The advantages of the microwave irradiation were avoidance of the self condensation of 2-[6-(ethynyl)pyridin-3-yl]-1*H*-benzimidazole, even without protection of the free benzimidazole NH and shorter reaction times together with excellent yields compared to conventional method (Changdev *et al.*, 2009). A microwave-enhanced, rapid, and efficient solid phase version of the Sonogashira reaction is presented. It has been applied to the coupling of aryl iodides and bromides with various acetylene derivatives giving excellent yields in 15-25 min. The scopes of homogeneous, solventless, and solid-phase conditions for Sonogashira coupling of aryl halides are compared (Erdélyi and Gogoll, 2001).

Quantum chemical calculation is the application of chemical, mathematical and computational skills to the approximations of chemistry problems (Hinsen, 2000). It uses computers to generate information such as properties of structure and dynamic molecular system. It also helps predict before running the actual experiments so that they can be better prepared for making observations. Theoretical studies are an important to approximate the electronic structure determinations, geometry optimizations, frequency calculations, transition structures, protein calculations, electron and charge distributions, etc with common computer software. In addition, the experimental cannot be explained with the electron term. Computational quantum chemistry is one of the challenging tasks in calculating the electronic structure and predicting properties of variety of molecules. This approach can be provided molecular models and guide the design of novel molecules (Esward and Sokhan, 2006).

Suramitr *et al.* (2010) shown that the electronic excitation transitions of carbazole-based oligomers, can be investigated using density functional theory (DFT) and time-dependent (TD) DFT methods. Absorption and fluorescence energies have been obtained from TD-B3LYP/SVP calculations performed on the S_1 optimized geometries and are in excellent agreement with experimental data. They conclude by discussing the benefits of theoretical calculations, which can provide critical structural and electronic understanding of excitation–relaxation phenomena that can be exploited in design of novel optical materials.

Tomasi *et al.* (2005) indicated that the solvent effects on the absorption and emission spectra are also relevant; therefore, we estimated the solvent effect on electronic spectra with a continuum solvent model in this study. The polarizable continuum model (PCM) is one of the most common and effective models among theoretical methods for considering solvent effects.

Suramitr *et al.* (2011) shown that photophysical properties and photoisomerization of 1,4-dimethoxy-2,5-bis[2-(thien-2-yl)ethenyl] benzene (DMTB) have been investigated for the EE-, EZ- and ZZ- stereoisomers by using DFT calculations. Absorption and fluorescence spectra of three isomers were analyzed by the symmetry-adapted cluster-configuration interaction (SAC-CI) and time-dependent density functional theory (TDDFT) method. The S_0 and S_1 state geometries were calculated by the DFT/TDDFT-(M06HF) method, and the calculated S_0 structures of the *EE-* and *ZZ-* isomers agree well with those of the X-ray structures. The geometry relaxation in the S_1 state was interpreted with regard to the excitation character. The results show that the photophysical properties of DMTB can be controlled with the conformation constraint and also indicate the possibility of photo functional molecular device such as switching function.

MATERIALS AND METHODS

Materials

1. Chemicals

    1.1   1-Bromopyrene ($C_{16}H_9Br$, Aldrich)

    1.2   2-Bromofluorene ($C_{13}H_9Br$, Aldrich)

    1.3   4-Bromobiphenyl ($C_{12}H_9Br$, Aldrich)

    1.4   1-Ethynyl-4-methylbenzene ($CH{\equiv}CC_6H_4CH_3$, Aldrich)

    1.5   4-Ethynyl-*N*,*N*-dimethylaniline ($CH{\equiv}CC_6H_4N(CH_3)_2$, Aldrich)

    1.6   Bis(triphenylphosphine)palladium(II)dichloride ($PdCl_2(PPh_3)_2$, Aldrich)

    1.7   Copper(I) iodide (CuI, Aldrich)

    1.8   Acetonitriel (CH_3CN, A.R. grade, ACI Labscan)

    1.9   Dichloromethane (CH_2Cl_2, A.R. grade, ACI Labscan)

    1.10 Dimethyl sulfoxide ($(CH_3)_2SO$, A.R. grade, ACI Labscan)

    1.11 Ethyl acetate ($C_4H_8O_2$, A.R. grade, ACI Labscan)

    1.12 Ethyl alcohol (C_2H_6O, A.R. grade, ACI Labscan)

    1.13 n-Hexane (C_6H_{14}, A.R. grade, ACI Labscan)

    1.14 Tetrahydrofuran (C_4H_8O, A.R. grade, ACI Labscan)

    1.15 Triethylamine ($C_6H_{15}N$, A.R. grade, ACI Labscan)

    1.16 Ammonium chloride (NH_4Cl, A.R. grade, ACI Labscan)

    1.17 Sodium sulfate (Na_2SO_4, A.R. grade, ACI Labscan)

    1.18 Silica gel

2. Instruments

2.1   Nuclear magnetic resonance (VARIAN $^{\text{UNITY}}$ INOVA spectrometer 400.00 MHz)

2.2   Fourier Transform Infrared Spectrophotometer (Bruker Equinox 55)

2.3   UV-Visible-Near IR Spectrometer (Jasco V-670)

2.4   Luminescence spectrophotometer (Perkin Elmer Instruments LS55)
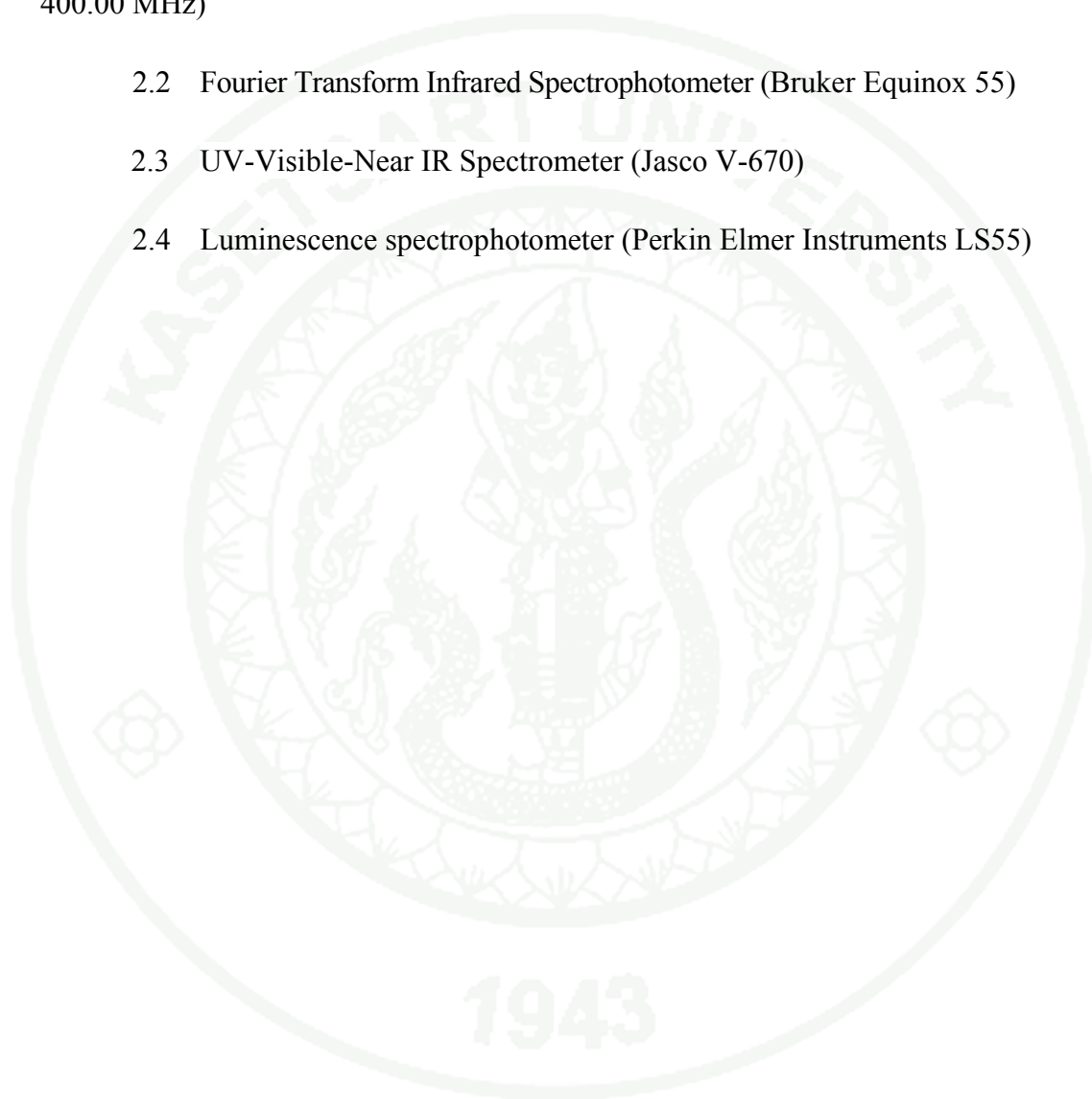
Methods

Method of experimentation

    1.   Synthesis

        1.1   1-ethynyl-4-methylbenzene derivative with the respective bromoarenes nucleus

$$R\!-\!Br \;+\; HC\!\equiv\!\!\!-\!\!\!\bigcirc\!\!\!-\!CH_3 \xrightarrow[\substack{DCM(THF),\,Et_3N \\ MW}]{PdCl_2(PPh)_3,\;CuI} R\!-\!\!\!\equiv\!\!\!-\!\!\!\bigcirc\!\!\!-\!CH_3$$

1-3   A

R =

          1   2   3
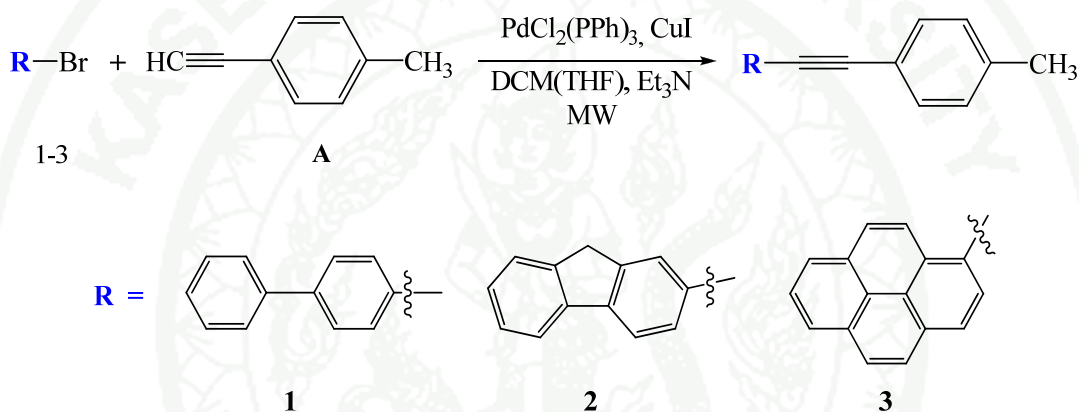
        Compound 1-3**A** were prepared by microwave-assisted Sonogashira coupling reaction. A mixture of bromoarene (1.00 mmol), 1-ethynyl-4-methylbenzene (0.1301 g., 1.12 mmol), $PdCl_2(PPh_3)_2$ (0.0149 g., 0.020 mmol), CuI (0.0040 g., 0.020 mmol), dichloromethane or tetrahydrofuran 3 mL and triethylamine 3 ml were mixed in a sealed 20 mL microwave vial. The reaction mixture was stirred at 340 W under microwave irradiation for 15 min or until disappearance of the starting material as monitored by thin layer chromatography. The cooled reaction mixture was washed with a saturated solution of ammonium chloride (2 × 15 mL) and water (2 × 15 mL). The combined organic layer was dried with anhydrous Na_2SO_4 and filtered. The solvent was removed in vacuum. The compound was purified by column chromatography (silica gel, Hexane/ dichloromethane).

1.2   Synthesis of 4-Ethynyl-*N*,*N*-dimethylaniline derivative with the respective bromoarenes nucleus
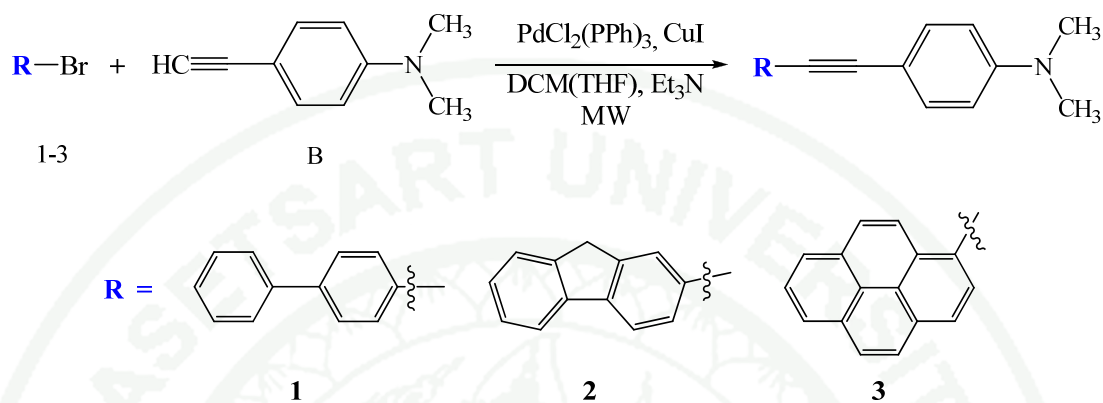
Compound 1-3**B** were prepared by microwave-assisted Sonogashira coupling reaction. A mixture of bromoarene (1.00 mmol), 4-Ethynyl-*N*,*N*-dimethylaniline (0.1626 g., 1.12 mmol), $PdCl_2(PPh_3)_2$ (0.0149 g., 0.020 mmol), CuI (0.0040 g., 0.020 mmol), dichloromethane or tetrahydrofuran 3 mL and triethylamine 3 ml were mixed in a sealed 20 mL microwave vial. The reaction mixture was stirred at 340 W under microwave irradiation for 15 min or until disappearance of the starting material as monitored by thin layer chromatography. The cooled reaction mixture was washed with a saturated solution of ammonium chloride (2 × 15 mL) and water (2 × 15 mL). The combined organic layers were dried with anhydrous Na_2SO_4, filtered, and the solvent was removed in vacuum. The compound was purified by column chromatography (silica gel, Hexane/ dichloromethane).

2.   Characterizations

FT-IR analyses were carried out using a Bruker FT-IR-spectrometer Equinox 55. The spectra were measured between 4000-400 cm^{-1} with the resolution of better than 0.5 cm^{-1}, using KBr disk method. The solid samples for FT-IR were ground with KBr, dried at 120 $^{\circ}$C and hydrolic-pressed.

^{1}H-NMR analyses were carried out using a VARIAN $^{\text{UNITY}}$ INOVA spectrometer which was operated at 400.00 MHz for ^{1}H-NMR. The compounds were dissolved in deuterated chloroform (CDCl$_3$) with tetramethysilane (TMS) as an internal reference.

3.   Photophysical Properties

UV-Vis analyses were done with a Jasco V-670 UV-VIS-NIR Spectrophotometer, using a quartz cell with 1 cm path length. The spectra were measured between 250-500 nm.

Fluorescence analyses were obtained using a Perkin Elmer Instruments LS55 fluorescence spectrophotometer using a quartz cell with 1 cm path length. The excitation wavelength for 1**A**, 2**A**, 3**A**, 1**B**, 2**B** and 3**B** were -, 336, 386, 347, 349 and 390 nm, respectively.

All compound solutions for UV-Vis spectra and fluorescence measurements were prepared at the concentration of 10 μM in several solvents, hexane, ethyl acetate, dichloromethane, ethyl alcohol, acetonitrile and dimethyl sulfoxide.

Methods of calculations

Quantum chemical calculation is the application of chemical, mathematical and computational skills to the approximations of chemistry problems. Quantum chemical calculation uses computers to generate information such as properties of structure and dynamic molecular system. It also helps predict before running the actual experiments so that they can be better prepared for making observations. This approach can be provided molecular models and guide the design of novel molecules.

1. Model of calculation

Starting geometries of 1-ethynyl-4-methylbenzene and 4-ethynyl-*N,N*-dimethylaniline derivatives consisting of 4-(biphenyl-4-ylethynyl)-methylbenzene (1**A**), 4-(biphenyl-4-ylethynyl)-*N,N*-dimethylaniline (1**B**), 4-((4aH-fluoren-7-yl)ethynyl)-methylbenzene (2**A**), 4-((4aH-fluoren-7-yl)ethynyl)-*N,N*-dimethylaniline (2**B**), 4-(pyren-1-ylethynyl)-methylbenzene (3**A**), 4-(pyren-1-ylethynyl)-*N,N*-dimethylaniline (3**B**) were constructed by molecular modeling. The structures of all molecules were shown in Figure 6.

2. Ground and Excited states Calculations.

The ground state and excited states geometries of their molecules were determined by a full optimization using the density functional theory (DFT) and time-depend density functional theory (TDDFT) level, respectively. The DFT calculations were performed with three different functionals to examine functional dependence. Standard hybrid functionals B3LYP and PBE0 were employed in calculations. The CAM-(Coulomb-attenuating method) B3LYP (Yanai *et al.*, 2004) was also examined for taking account of the long-range corrections for describing the long π-conjugation. Standard exchange functionals may suffer from improper long-range description, in particular, for the electronic excited states of significantly different polarity between the ground and excited states. The basis set 6-311G(d,p) has been used for the geometries optimization. The electronic excitation energies and oscillator strengths

were calculated with using the TDDFT at the molecular structures optimized by the TDDFT. For simulating the absorption spectra and fluorescence spectra were examined.
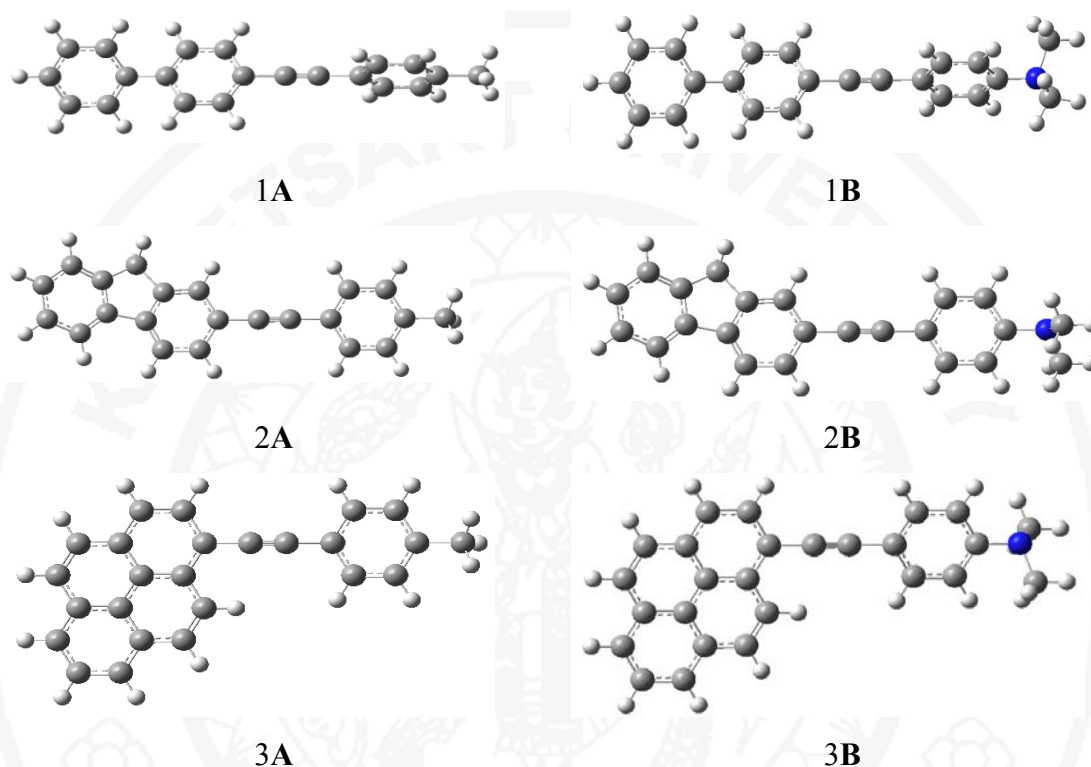
Figure 6 Schematic diagram of 1-ethynyl-4-methylbenzene (**A**) and 4-Ethynyl-*N*,*N*-dimethylaniline (**B**) derivatives.

The solvent effects on the absorption and emission spectra are also relevant; therefore, we estimated solvent effect on electronic spectra with a continuum solvent model in this study. The polarizable continuum model (PCM) is one of the most common and effective model among theoretical methods for considering solvent effects. There are two solvation schemes possible for calculating excitation energies using the methods based on the linear response (LR) and state-specific (SS) theory (shown in Figure 7).
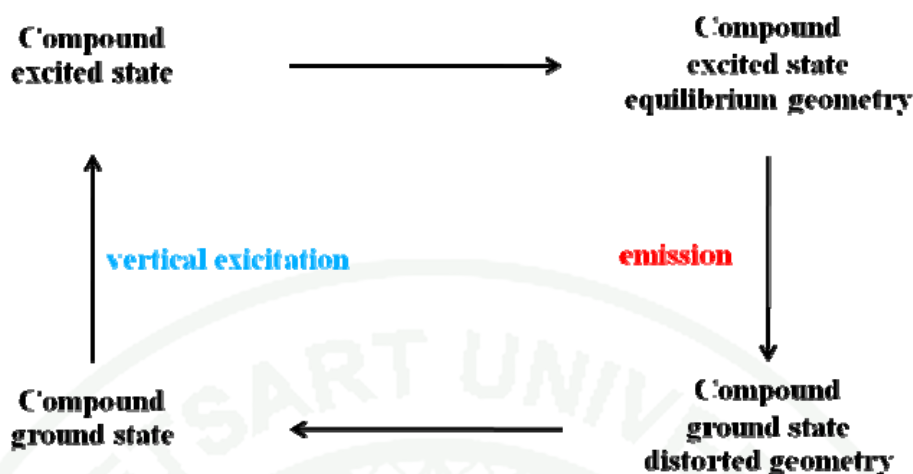
Figure 7 The schemes possible for calculating excitation energies.

The first scheme is the state-specific (SS) solvation in which the solvent polarization charges are determined by the electron density of solute in the specific excited state. Consequently, the calculations are nonlinear and each state is calculated by means of the self-consistent reaction field (SCRF) scheme. The second scheme is LR solvation in which solvent polarization charges are fixed in the ground state. Therefore, in the LR solvation scheme, the electron densities of excited states are not necessary and excitation energies can be calculated without additional iterations. It has been pointed out that the LR and SS schemes are intrinsically different for the solvent effect on excitation energies and the SS scheme is more reliable in principle. In this study we used both the SS and LR solvation schemes of the PCM in the TDDFT calculations.

For absorption, the molecular geometry in solution was optimized for the S_0 state with equilibrium solvation and the TDDFT calculations were performed with the SS and LR solvation schemes in nonequilibrium model. For emission, the S_1-state geometry in dichloromethane was optimized with equilibrium solvation and LR scheme. Then, the excitation energies were calculated with the SS and LR solvation schemes in nonequilibrium model. All calculations were performed using the GAUSSIAN09 suite (Scalmani and Frisch, 2010) of programs Revision B.01.

RESULTS AND DISCUSSION

Experimentation

1. Synthesis and characterization

1.1 1-ethynyl-4-methylbenzene derivatives

1.1.1 4-(biphenyl-4-ylethynyl)-methylbenzene (1A)

Compound 1A was prepared from 1 (0.2331 g., 1.00 mmol), A (0.1301 g., 1.12 mmol), $PdCl_2(PPh_3)_2$ (0.0149 g., 0.020 mmol), CuI (0.0040 g., 0.020 mmol), dichloromethane or tetrahydrofuran 3 mL and triethylamine 3 ml. 1(A) could not be synthesized by this method. However, in the future, this method will be improved for success in the new synthesis

1.1.2 4-((4aH-fluoren-7-yl)ethynyl)-methylbenzene (2A)

Compound 2A could be obtained as a white solid with 80% yield. The product appeared as blue-green solid under UV light (365 nm). In dichloromethane solvent, compound 2A gave colorless solution under visible light and light purple solution under UV light (365 nm) as show in Figure 8. ^1H-NMR spectra were shown in Figures 9 (400 MHz, δ from TMS (ppm), $CDCl_3$) and the following signal were observed: δ 2.38 (3H, s, H_A), 3.91 (2H, s, H_B), 7.17 (2H, d, H_C, J = 7.8 Hz), 7.32 (1H, t, H_D, J = 8.0 Hz), 7.38 (1H, t, H_E, J = 6.9 Hz), 7.44 (2H, d, H_F, J = 8.1 Hz), 7.51-7.64 (2H, m, H_{HG}), 7.71 (1H, s, H_I), 7.45 (1H, d, H_J, J = 7.9 Hz) and 7.78 (1H, d, H_K, J=7.4 Hz).

Solid   Solution

Visible light   UV light (365 nm)   Visible light   UV light (365 nm)
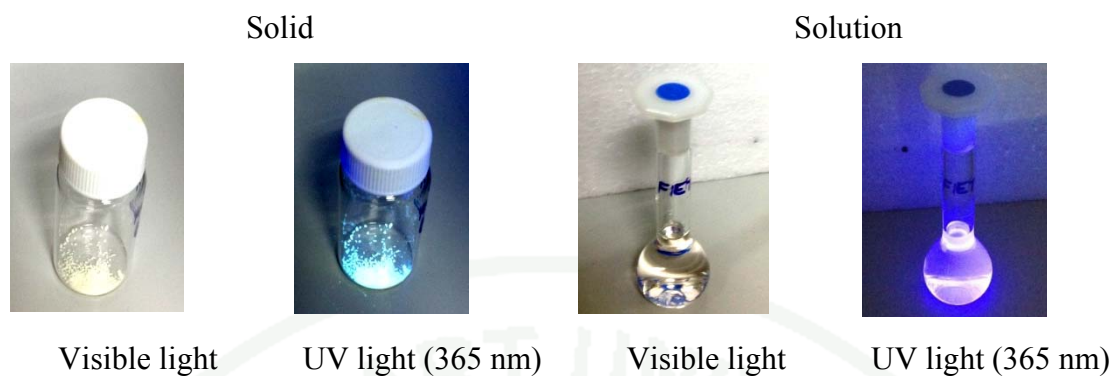
Figure 8 Physical appearance of 4-((4aH-fluoren-7-yl)ethynyl)-methylbenzene (**2A**) under visible light and UV light (365 nm).
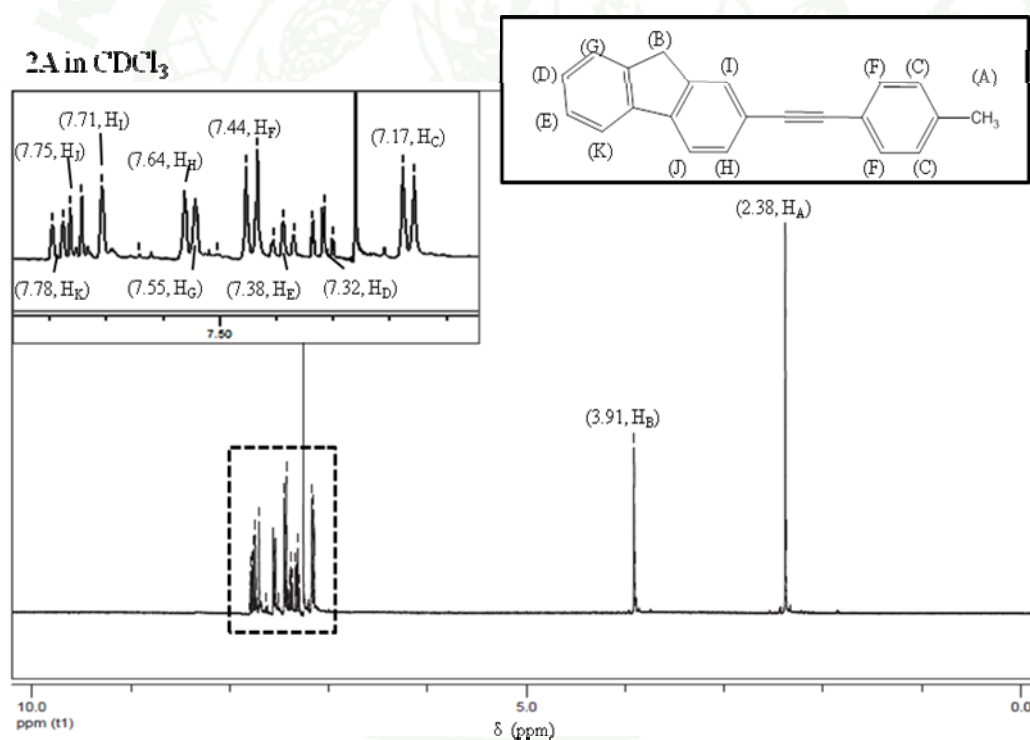
Figure 9 ^1H-NMR spectrum of 4-((4aH-fluoren-7-yl)ethynyl)-methylbenzene (**2A**) in CDCl$_3$. Inset : expansion of the region 6.50-7.40 ppm and molecular structure **2A**.

1.1.3   4-(pyren-1-ylethynyl)-methylbenzene (3**A**)

Compound 3**A** could be obtained as a yellow solid with 77% yield. The product appeared as blue-green solid under UV light (365 nm). In dichloromethane solvent, compound 3**A** gave colorless solution under visible light and light blue solution under UV light (365 nm) as show in Figure 10. ^{1}H-NMR spectra were shown in Figures 11 (400 MHz, δ from TMS (ppm), CDCl$_3$) and the following signal were observed: δ 2.42 (3H, *s*, H$_A$), 7.24 (2H, *d*, H$_B$, J = 8.0 Hz), 7.62 (2H, *d*, H$_C$, J = 8.2 Hz), 8.03 (1H, *t*, H$_D$, J = 7.6 Hz), 8.05 (1H, *d*, H$_E$, J = 8.9 Hz), 8.10 (1H, *d*, H$_F$, J = 8.9 Hz), 8.13 (1H, *d*, H$_G$, J = 8.0 Hz), 8.19 (1H, *d*, H$_H$, J = 9.1 Hz), 8.20 (2H, *d*, H$_I$, J = 7.9 Hz)   , 8.23 (1H, *d*, H$_J$, J = 7.7 Hz) and 8.67 (1H, *d*, H$_K$, J = 9.1 Hz).

	Solid		Solution	

Visible light	UV light (365 nm)	Visible light	UV light (365 nm)
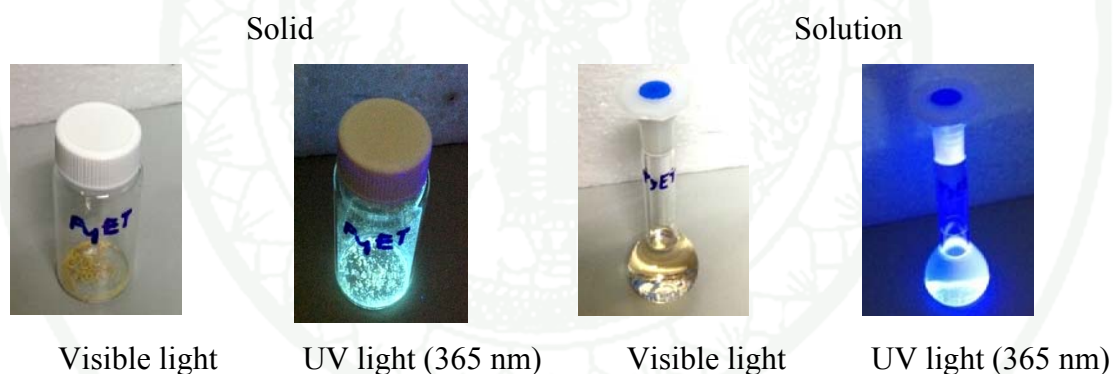
Figure 10 Physical appearance of 4-(pyren-1-ylethynyl)-methylbenzene (3**A**) under
visible light and UV light (365 nm).
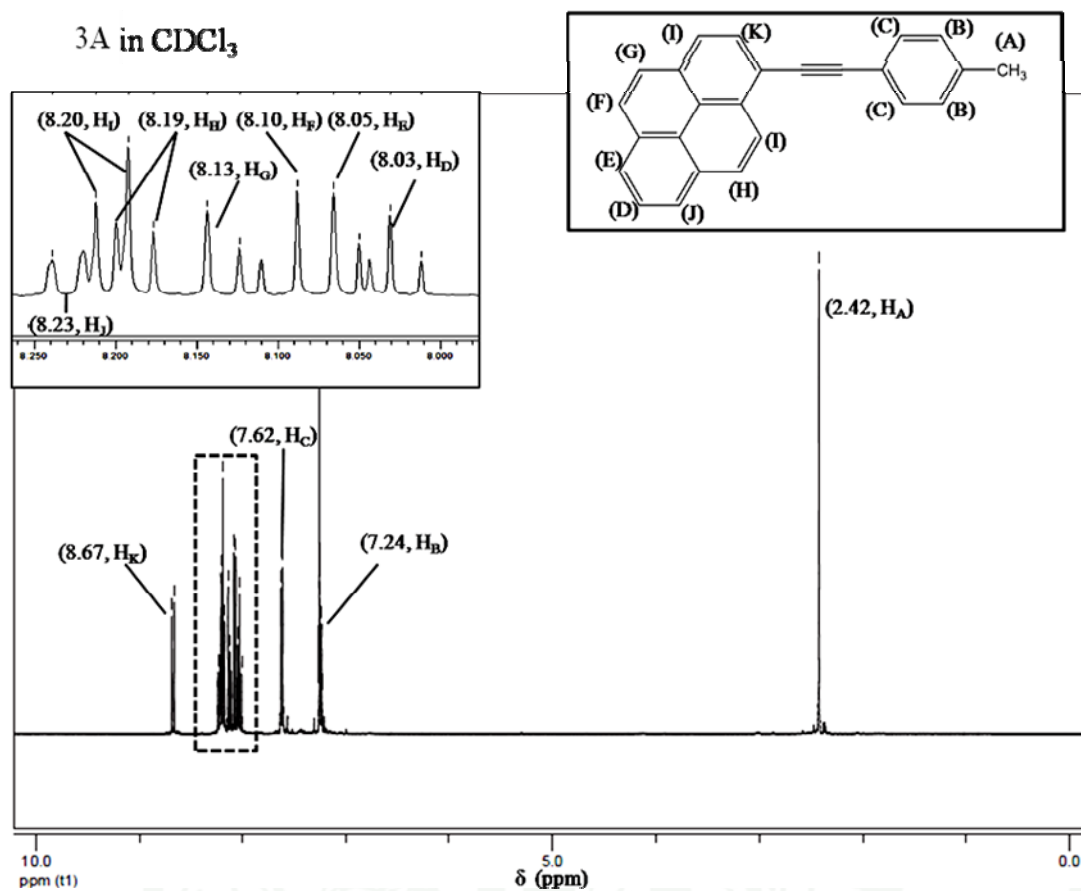
Figure 11 ^1H- NMR spectrum of 4-(pyren-1-ylethynyl)-methylbenzene (**3A**) in CDCl$_3$. Inset : expansion of the region 8.00-8.25 ppm and molecular structure **3A**.
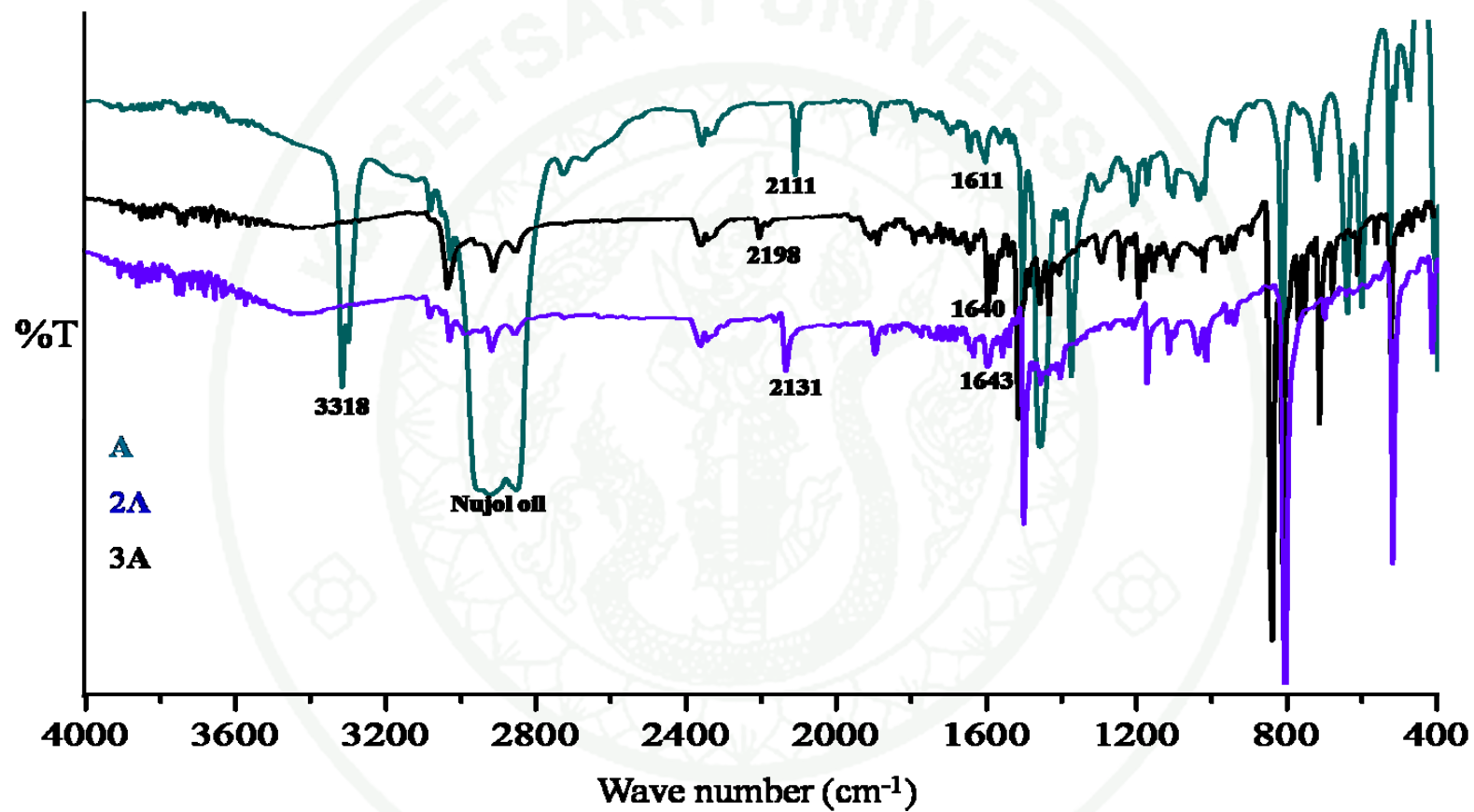
Figure 12 FT-IR spectra of 1-ethynyl-4-methylbenzene (**A**) in nujol oil and 4-((4aH-fluoren-7-yl)ethynyl)-methylbenzene (**2A**) and 4-(pyren-1-ylethynyl)-methylbenzene (**3A**) in KBr disks.

Table 2 Assignment of absorption bands observed in FT-IR spectra in Figure 12.

| Wave number (cm^{-1}) | | | Assignment |
A	2A	3A	(John, 2000)
3318(s)	-	-	$\equiv$C-H stretching
3020(m)	3025(m)	3033	=C-H stretching
2900-2850(b)	2914	2914	-C-H stretching
(Nujol oil)	2854(w)	2857(w)	-C-H stretching
2361	2362	2360	O=C (CO_2 region)
2111(s)	2131(s)	2198(s)	-C$\equiv$C- stretching
1611(m)	1640(m)	1643(m)	C=C stretching
1507(s)	1499(s)	1512(s)	C=C stretching
1458,1375	-	-	Nujol oil region
817(s)	809	839	para-disubstituted

FT-IR spectra of the reactant **A** and the products 2**A**, 3**A** were show in Figure 12. Typically, the reactant **A** showed characteristic absorptions at 3318 and 2111 cm^{-1}, corresponding to H-C$\equiv$ stretching and C$\equiv$C stretching, respectively. The bands at 3318 cm^{-1} was not observed in the spectra of the products and the bands at 2111cm^{-1} shifted to 2131 and 2198 cm^{-1} in the spectra of 2**A** and 3**A**, respectively, indicating that the reactant A was completely consumed and the products were formed. In addition, similar absorptions were observed in all spectra and were assigned as follows. The bands in the region 3100-3000 and 2960-2850 cm^{-1} were attributed to C-H stretching vibration of aromatic rings and methyl group, respectively. The absorptions in the region 2260-2100 and 1680-1500 cm^{-1} were consistent with C$\equiv$C and C=C stretching vibration, respectively. In the fingerprint region between (1600-400 cm^{-1}), para-disubstitution could also observed at 860-800 cm^{-1} (John, 2000). It was noted that weak absorption appeared at 2360 cm^{-1} due to C=O stretching vibration of carbon dioxide group (Gerakines *et al.*, 1995).

1.2 4-ethynyl-*N,N*-dimethylaniline derivatives

1.2.1 4-(biphenyl-4-ylethynyl)-*N,N*-dimethylaniline (1**B**)

Compound 1**B** could be obtained as a white solid with 93% yield. The product appeared as purplish blue solid under UV light (365 nm). In dichloromethane solvent, compound 1**B** gave colorless solution under visible light and light blue solution under UV light (365 nm) as show in Figure 13. *¹H*-NMR spectra were shown in Figures 14 (400 MHz, δ from TMS (ppm), CDCl₃) and the following signal were observed: δ 3.01 (6H, *s*), 6.70 (2H, *d*, J = 8.8Hz), 7.34 (1H, *t*, J = 7.3 Hz), 7.40-7.45 (4H, *m*), 7.57 (4H, *m*) and 7.61 (2H, *d*, H$_F$, J = 7.8 Hz).

Solid	Solution

Visible light	UV light (365 nm)	Visible light	UV light (365 nm)
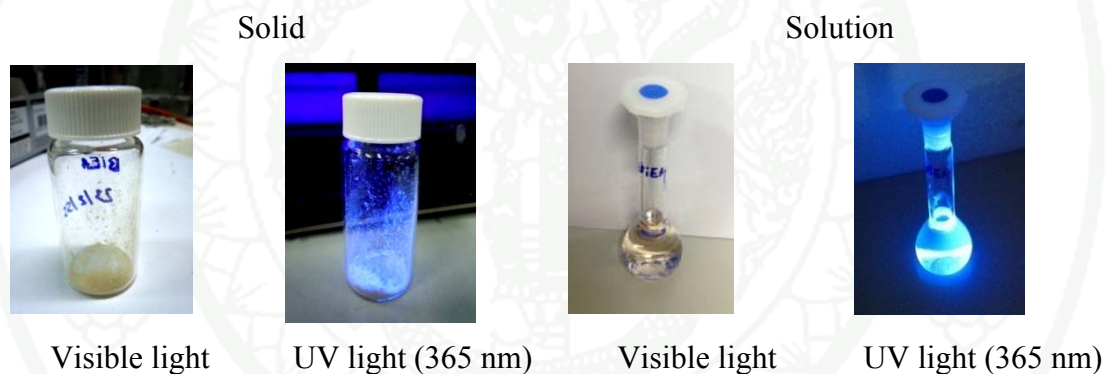
Figure 13 Physical appearance of 4-(biphenyl-4-ylethynyl)-*N,N*-dimethylaniline (1**B**) under visible light and UV light (365 nm).

Figure 14 ^1H-NMR spectrum of 4-(biphenyl-4-ylethynyl)-*N,N*-dimethylaniline (1**B**) in CDCl$_3$. Inset : expansion of the region 7.25-7.65 ppm and molecular structure 1**B**.

1.2.2 4-((4aH-fluoren-7-yl)ethynyl)-*N,N*-dimethylaniline (2**B**)

Compound 2**B** could be obtained as a white solid with 83% yield. The product appeared as purplish blue solid under UV light (365 nm). In dichloromethane solvent, compound 2**B** gave colorless solution under visible light and light purplish blue solution under UV light (365 nm) as show in Figure 15. ^1H-NMR spectra were shown in Figures 16 (400 MHz, δ from TMS (ppm), CDCl$_3$) and the following signal were observed: δ 3.00 (6H, *s*, H$_A$), 3.90 (2H, *s*, H$_B$), 6.68 (2H, *d*, H$_C$, J = 8.7 Hz), 7.32 (1H, *t*, H$_D$, J = 8.0 Hz), 7.38 (1H, *t*, H$_E$, J = 7.8 Hz), 7.43 (2H, *d*, H$_F$, J = 8.9 Hz), 7.52-7.55 (2H, *m*, H$_{HG}$), 7.68 (1H, *s*, H$_I$), 7.73 (1H, *d*, H$_J$, J = 7.9 Hz) and 7.77 (1H, *d*, H$_K$, J=7.5 Hz).

Figure 15 Physical appearance 4-((4aH-fluoren-7-yl)ethynyl)-*N,N*-dimethylaniline
(2**B**) under visible light and UV light (365 nm).

Figure 16 *¹H*-NMR spectrum of 4-((4aH-fluoren-7-yl)ethynyl)-*N,N*-dimethylaniline
(2**B**) in CDCl₃. Inset : expansion of the region 7.20-7.80 ppm and
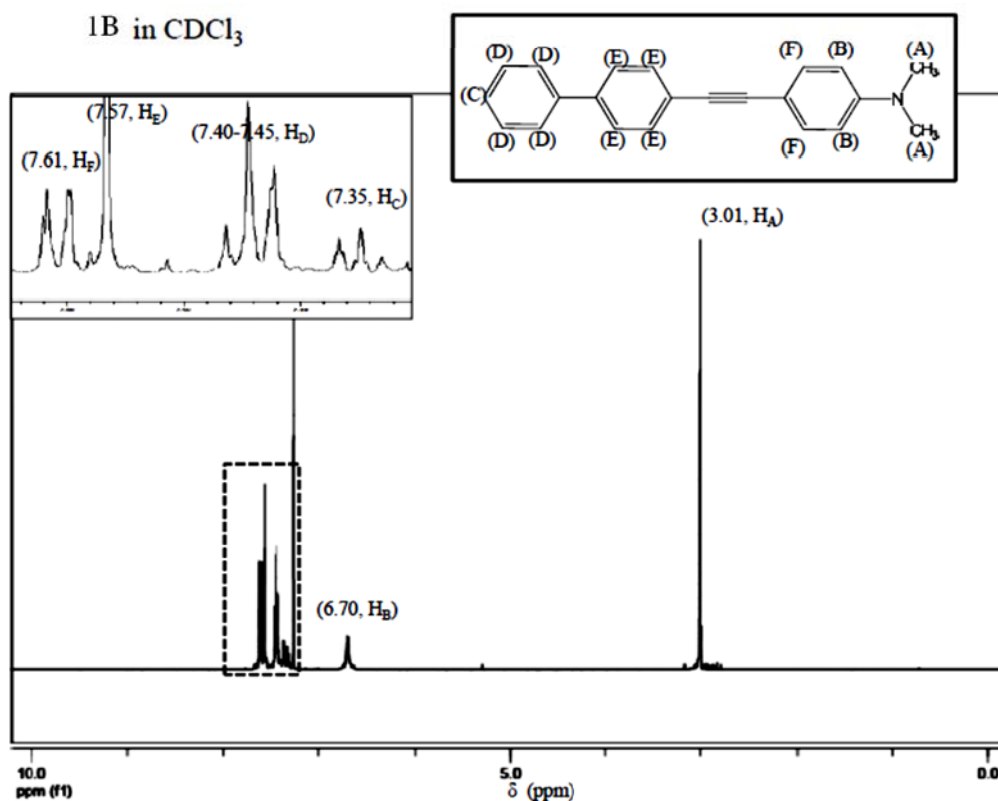molecular structure 2**B**.

1.2.3 4-(pyren-1-ylethynyl)-*N,N*-dimethylaniline (3**B**)

Compound 3**B** could be obtained as a bright yellow solid with 79% yield. The product appeared as green solid under UV light (365 nm). In dichloromethane solvent, compound 3**B** gave yellow solution under visible light and light green solution under UV light (365 nm) as show in Figure 17. ^{1}H-NMR spectra were shown in Figures 18 (400 MHz, δ from TMS (ppm), CDCl$_3$) and the following signal were observed: δ 3.04 (6H, *s*, H$_A$), 6.74 (2H, *d*, H$_B$, J = 8.9 Hz), 7.60 (2H, *d*, H$_C$, J = 8.9 Hz), 8.03 (1H, *t*, H$_D$, J = 7.6 Hz), 8.04 (1H, *d*, H$_E$, J = 8.9 Hz), 8.07 (1H, *d*, H$_F$, J = 9.0 Hz), 8.11 (1H, *d*, H$_G$, J = 8.0 Hz), 8.17 (1H, *d*, H$_H$, J = 9.2 Hz), 8.18 (1H, *d*, H$_I$, J = 7.9 Hz), 8.19 (1H, *d*, H$_J$, J = 6.8 Hz), 8.21 (1H, *d*, H$_K$, J = 7.8 Hz) and 8.69 (1H, *d*, H$_L$, J = 9.1 Hz).

Solid		Liquid	
Visible light	Long-light (UV)	Visible light	Long-light (UV)
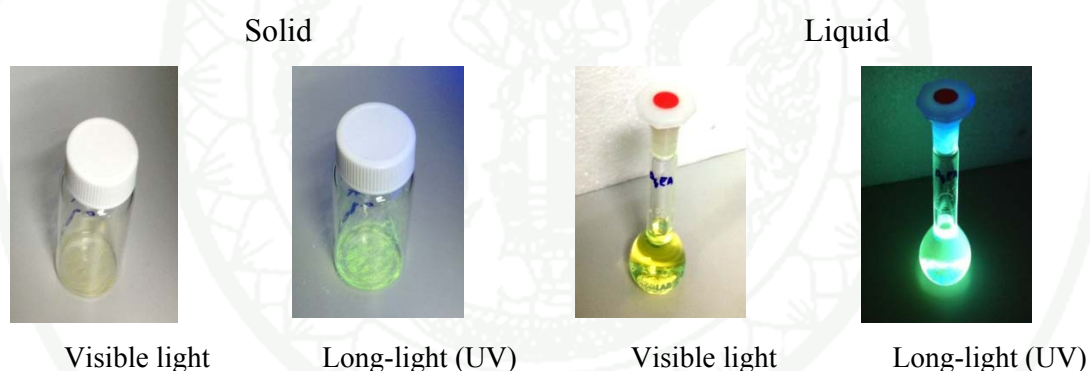
Figure 17 Physical appearance 4-(pyren-1-ylethynyl)-*N,N*-dimethylaniline (3**B**) under visible light and UV light (365 nm).
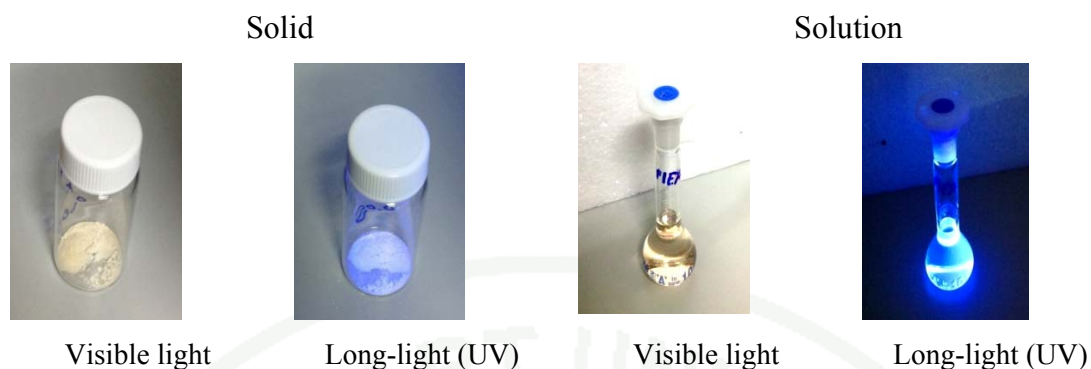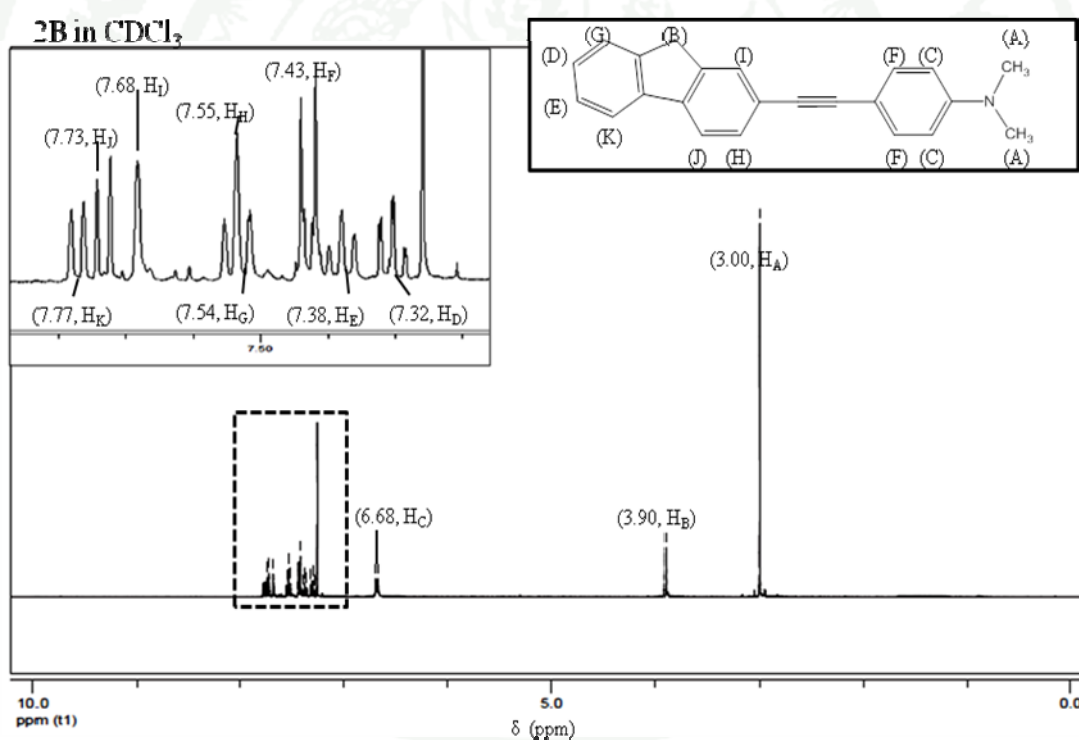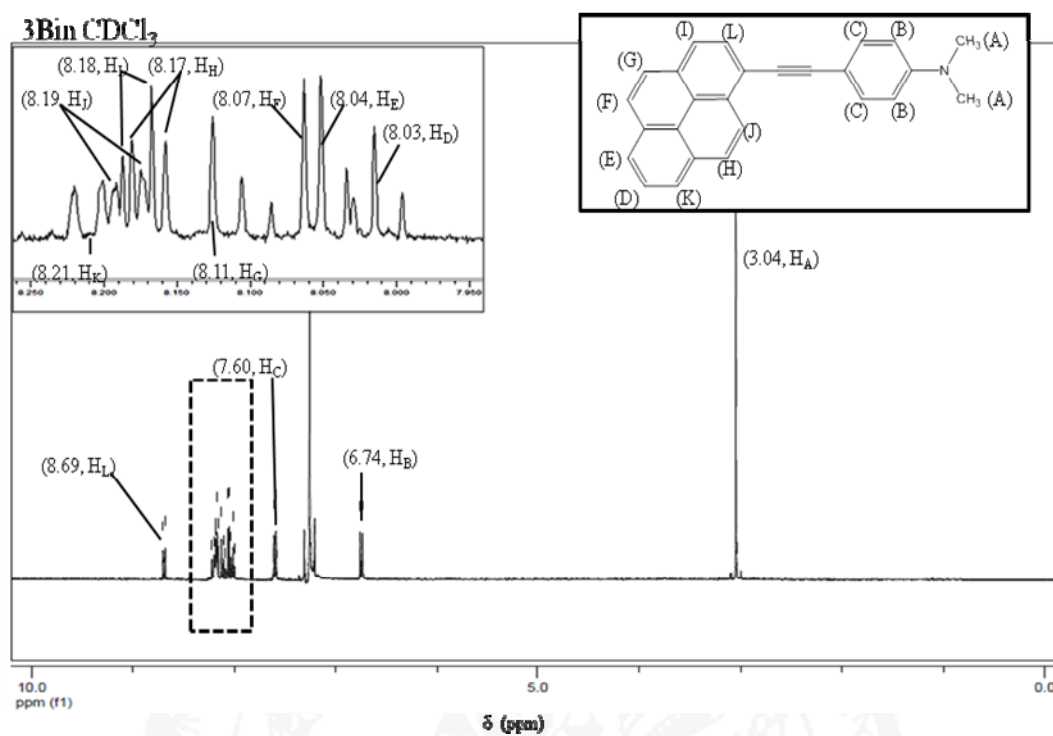
Figure 18 ^1H-NMR spectrum of 4-(pyren-1-ylethynyl)-*N,N*-dimethylaniline (3**B**) in CDCl₃. Inset : expansion of the region 7.95-8.25 ppm and molecular structure 3**B**.
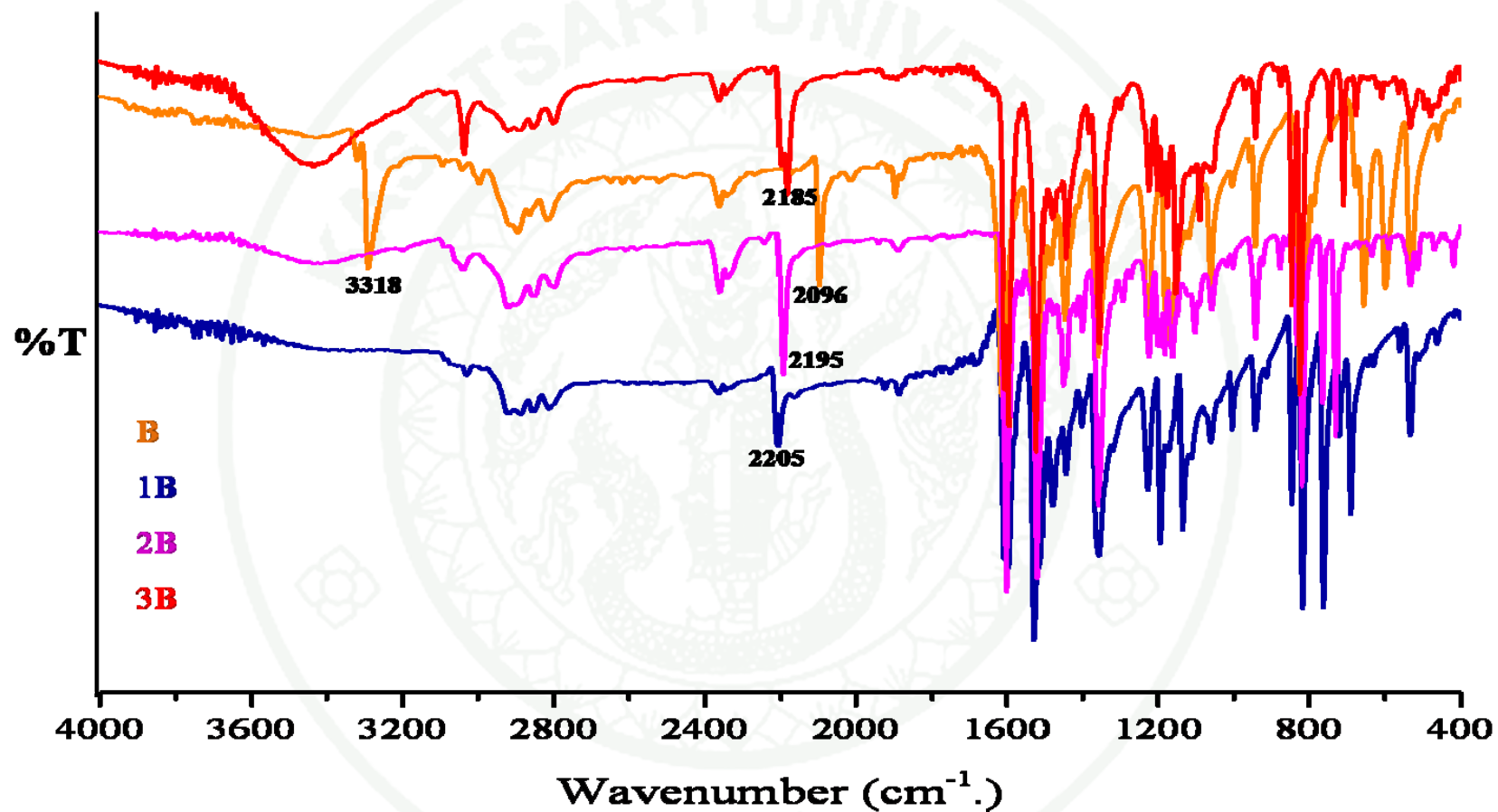
Figure 19 The FT-IR spectrum of 4-ethynyl-*N,N*-dimethylaniline (**B**), 4-(biphenyl-4-ylethynyl)-*N,N*-dimethylaniline (1**B**),
4-((4aH-fluoren-7-yl)ethynyl)-*N,N*- dimethylaniline (2**B**) and 4-(pyren-1-ylethynyl)-*N,N*-dimethylaniline (3**B**)
in KBr disks.

Table 3 Assignment of absorption bands observed in FT-IR spectra in Figure 19.

	Wavenumber (cm^{-1})			Assignment
B	1**B**	2**B**	3**B**	(John, 2000)
3318(s)	-		-	$\equiv$C-H stretching
3020(m)	3034(m)	3030(m)	3036(m)	=C-H stretching
2898(m)	2924(m)	2912(m)	2925(m)	-C-H stretching
2805(w)	2863(w)	2839(w)	2852(w)	-C-H stretching
2360	2368	2357	2365	O=C (CO$_2$ region)
2096(s)	2205(s)	2195(s)	2185(s)	-C$\equiv$C- stretching
1610	1600	1600	1595	C=C stretching
1520(s)	1521(s)	1518(s)	1522(s)	C=C stretching
1358	1357	1356	1356	C-N stretching
818(s)	812(s)	821(s)	821(s)	para-disubstitued

The FT-IR spectrum of the reactant **B** shows the interesting peaks at 3318 and 2096 cm^{-1} corresponding to the H-C$\equiv$ stretching and C$\equiv$C stretching, respectively. The reactant **B** was used in order to form the products. In the FT-IR spectra of 1**B**, 2**B** and 3**B**, the peak of product at 3318 cm^{-1} disappeared and the C$\equiv$C stretching was shifted to 2195 cm^{-1} due to coupling reaction. The loss of the H-C$\equiv$ stretching vibration and the shift of **C$\equiv$C** stretching were the evidences that 1**B**, 2**B** and 3**B** were successfully synthesized by microwave-assisted Sonogashira coupling. In addition, similar absorptions were observed in all spectra and assigned as the following. The bands in the region ~3030 and 2925-2800 cm^{-1} were attributed to C-H stretching vibration of aromatic rings and methyl group, respectively. The absorptions in the region ranging from 2205-2096 and 1610-1518 cm^{-1} were consistent with C$\equiv$C and C=C stretching vibrations, respectively. The peak in the region ~1357 cm^{-1} could

be assigned as C-N stretching vibration of dimethylamine group. In the fingerprint region between (1600-400 cm^{-1}), para-disubstitution could be also observed at 860-800 cm^{-1} (John, 2000). It should be noted that weak absorption appeared at 2360 cm^{-1} as the result of C=O stretching vibration of carbon dioxide group (Gerakines *et al.*, 1995).

The results showed that all compounds were obtained by the Pd catalytic cross-coupling of 1-ethynyl-4-methylbenzene and 4-Ethynyl-*N,N*-dimethylaniline derivatives with corresponding bromoarene in satisfactory to high yields using Sonogashira coupling, microwave-assisted synthesis. In all the compounds, when stimulated by UV light (365 nm), they can response in the light both in solid and liquid states. Moreover, all compounds were characterized by *^{1}H*-NMR and FT-IR techniques.

2. Photophysical properties

2.1 Absorption spectra

The absorption spectra of the prepared compounds in dichloromethane were shown in Figure 20 and 21. The wavelengths at which absorption was maximum wavelength summarized in Table 4.
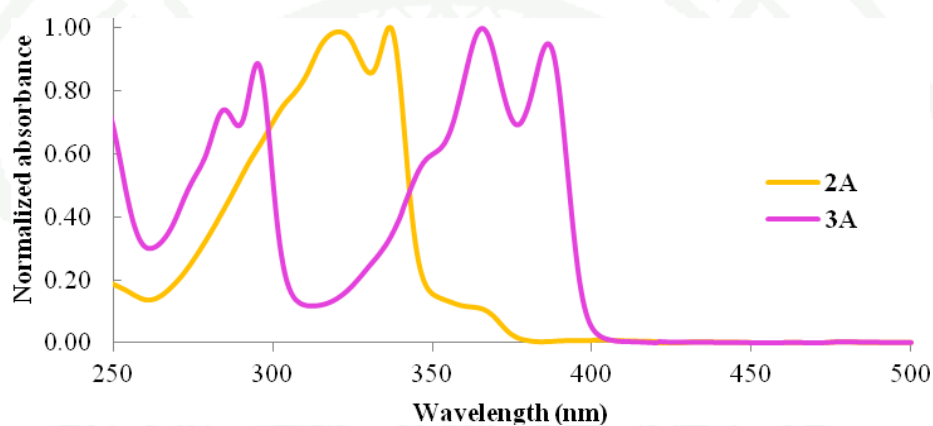
Figure 20 Absorption spectra of 1-ethynyl-4-methylbenzene derivatives 2**A** and 3**A** in dichloromethane.
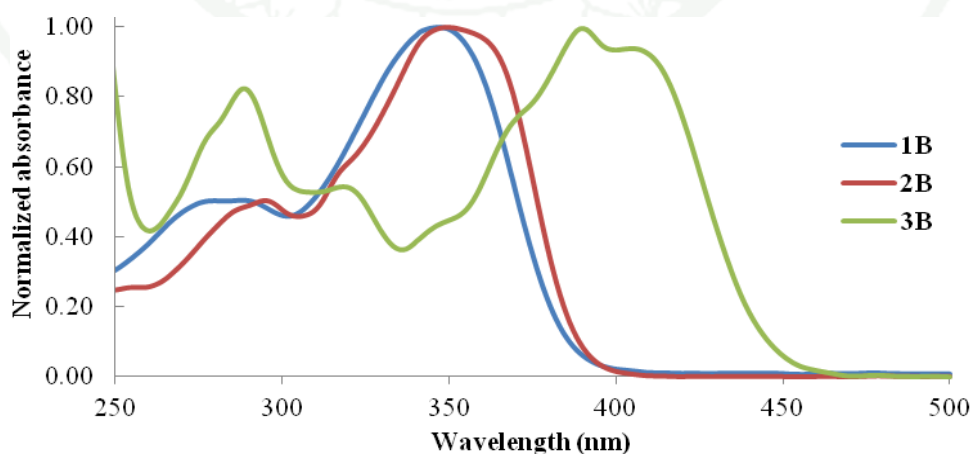
Figure 21 Absorption spectra of 4-ethynyl-*N,N*-dimethylaniline derivatives 1**B**, 2**B** and 3**B** in dichloromethane.

2.2 Emission spectra

The emission spectra of the prepared compounds in dichloromethane were shown in Figure 22 and 23. The wavelengths at which absorption was maximum wavelength summarized in Table 4.
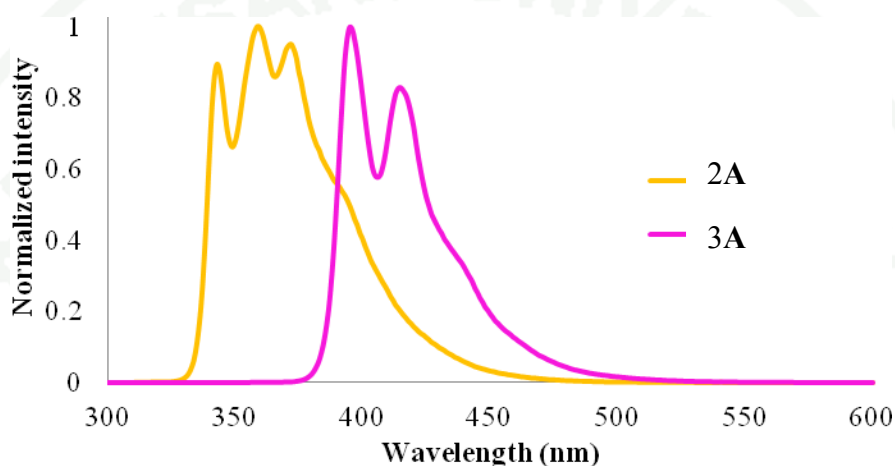
Figure 22 Emission spectra of 1-ethynyl-4-methylbenzene derivatives, 2**A** and
3**A** in dichloromethane.
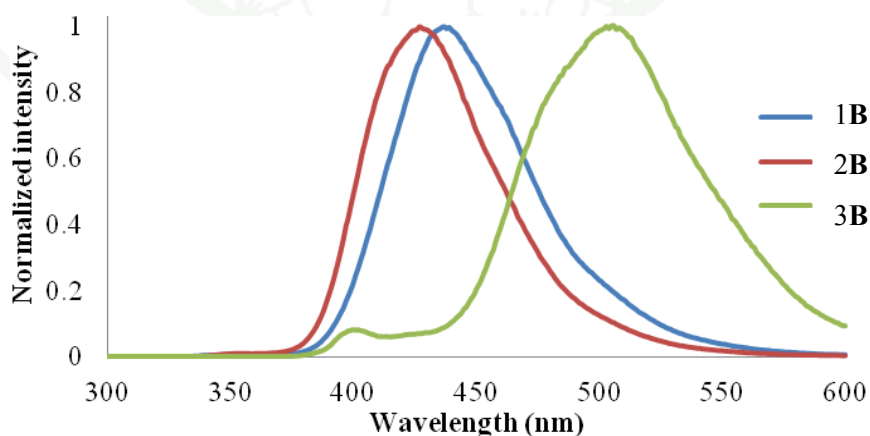
Figure 23 Emission spectra of 4-ethynyl-*N*,*N*-dimethylaniline derivatives, 1**B**, 2**B**
and 3**B** in dichloromethane.

Table 4 Photophysical data of all compounds in dichloromethane solution.

Compound	Absorption λmax (nm) [v/cm⁻¹]	Emission λmax (nm) [v/cm⁻¹]	Stock shift λmax (nm) [Δv/cm⁻¹]
2A	320 [31,250]	343 [29,155]	23 [2,095]
	336 [29,762]	359 [27,855]	23 [1,907]
3A	365 [27,398]	395 [25,316]	30 [2,082]
	386 [25,907]	415 [24,096]	29 [1,811]
1B	347 [28,818]	437 [22,883]	90 [5,935]
2B	349 [28,653]	427 [23,419]	78 [5,234]
3B	390 [25,641]	506 [19,763]	116 [5,878]

The absorption spectra of all compounds recorded in dichloromethane are displayed in Figures 20 and 21, and the data are reported in Table 4. The biphenyl (1) and fluorene (2) derivative compounds show the close wavelength absorption due to biphenyl (1) and fluorene (2) derivatives should have an equal conjugated systems, while the pyrene (3) derivatives possessed the longest wavelength due to that more conjugated systems. The more delocalization there is, the smaller the gap between the HOMO and the LUMO will become. To promote an electron therefore takes less energy in pyrene (3) derivatives because the gap between the levels is less that less energy means a lower frequency of light gets absorbed and that's equivalent to a longer wavelength (Jim, 2007). The observed pattern for the absorption spectrum of 3**A** is similar to 1-bromopyrene (Appendix Figure 1), but the peak position is more red shift compared to 1-bromopyrene. Moreover, the red shift is attributed to the extension of conjugation on replacement of the arenes group with 1-ethynyl-4-methylbenzene unit, that is, efficient π-conjugation. While the group of compounds that contained 4-ethynyl-*N,N*-dimethylaniline (**B**) could broaden the absorption peaks better, the absorption peaks of the group of compounds that contained 1-ethynyl-4-

methylbenzene (**A**) could not broaden due to charge transfer transition from the amine donor to the arenes acceptor (Nantalaksakul *et al.*, 2009). Moreover, the group (**B**) compounds clearly exhibited the absorption spectra of that have higher wavelength than of group (**A**) compounds.

The emission spectra recorded for all compounds in dichloromethene are displayed in Figures 22 and 23 (the data are collected in Table 4). All compounds are intensely emitting in the violet to light green region when exposed to ultraviolet light. The emission wavelengths of the compounds are in the order 2**A** < 3**A** < 2**B** < 1**B** < 3**B**. The emission profile of 3**A** is similar to that observed from 1-(phenylethynyl)-pyrene (392 nm) (Liu *et al.*, 2008), due to extended π-system in the electronic excitation. This is largely in keeping with the trend in the conjugation length present in the molecules (Thomas *et al.*, 2012).

Emission spectra of 4-ethynyl-*N,N*-dimethylaniline derivatives compounds are red shift similar to that observed for 1-ethynyl-4-methylbenzene derivatives compounds due to the efficient charge transport supported by strong electronic coupling between the donor and acceptor through C-C triple bond brings down the HOMO-LUMO energy gap and emits visible light (Ho *et al.*, 2005). The amine of the 4-ethynyl-*N,N*-dimethylaniline-functionalized also caused the significant red-shifts of emission wavelength resulting from the relaxation of a polarized excited state before emission (Hancock *et al.*, 2006). In addition, the compounds 1**B** and 2**B** showed the similar absorption wavelengths. The emission wavelength of 1**B** was higher than 2**B** because the structure of 1**B** was less rigid than 2**B**. Therefore, the more flexible compound 1**B** could vibrate and lose the energy in the form of heat so the energy gap lessened and emission wavelength increase (Kordas and El-Bayoumi, 1974).

2.3 Strokes shift

The Strokes Shift of the prepared compounds in dichloromethane are shown in Figure 24 and the data are collected in Table 4. The emission of 4-ethynyl-*N,N*-dimethylaniline derivatives compounds showed larger strokes shift compared with those observed for 1-ethynyl-4-methylbenzene derivatives compounds. It was assumed to be the consequence in substantial change in the geometrical structure from the ground state (S_0) to the first excited state (S_1) (Baathulaa *et al.*, 2010). The amine containing compounds (1-3)**B** point to the existence of non-radiative relaxation pathways in these molecules.
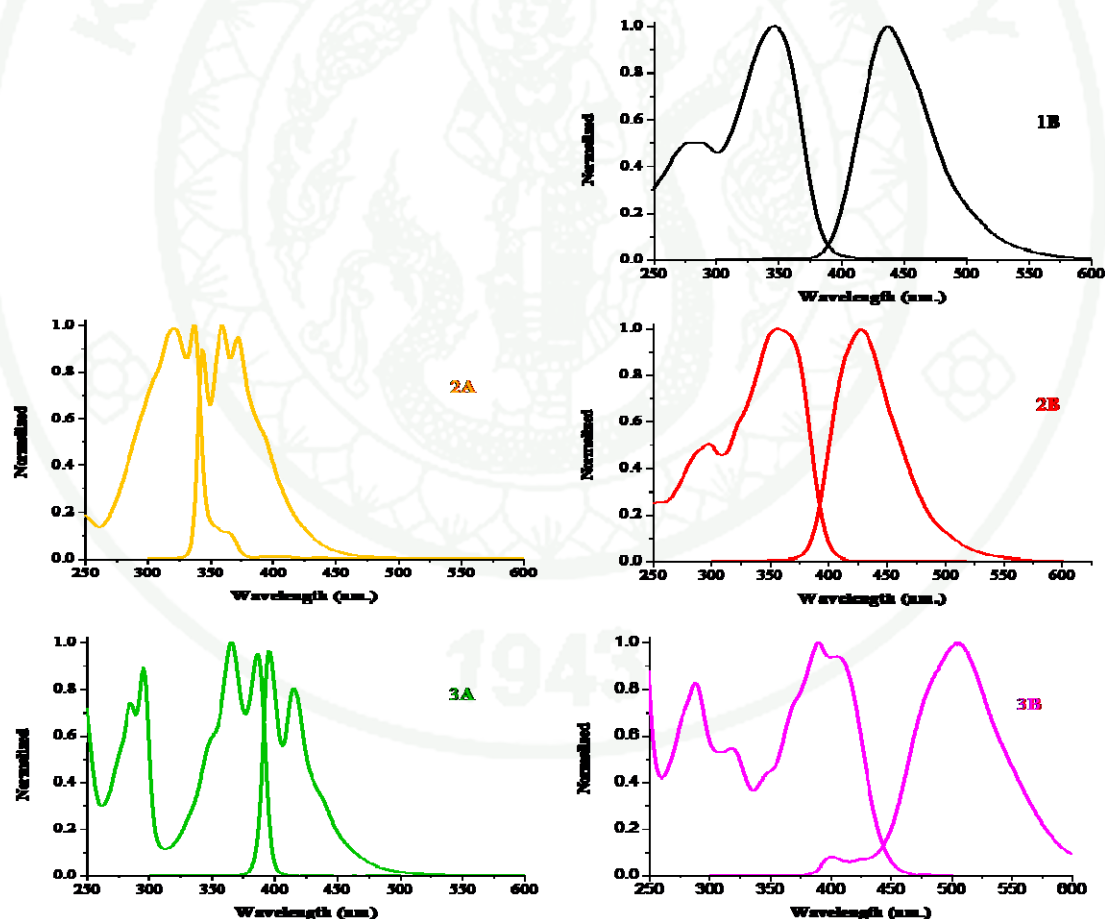
Figure 24 Absorption and emission spectra of 2**A**, 3**A** derivatives and 1**B**, 2**B**, 3**B** derivatives in dichloromethane.

2.4 Solvatochromic effect

Solvatochromic behavior was differences in absorption wavelength of molecule in solvents with different polarity. Changes in absorption wavelength arised as a result of an interaction between the solute and solvent molecules (Zakerhamidi M. S *et al.*, 2012). Strong solvatochromic behavior could be observed for molecules possessing large dipole moment changes during transition between two electronic states.

The solvatochromism study was carried out in this work. All prepared compounds were dissolved in different solvents to evaluate the effect of solvent polarity on both absorption and emission properties. The solvents used were hexane (Hex), ethyl acetate (EtOAc), dichloromethene (DCM), acetonitrile (ACN) and dimethyl sulfoxide (DMSO). The optical image, absorption, and emission spectra of each compound in the various solvents were shown in Appendix Figure A2-A6 and the data were collected in Table 5 and 6.

Compounds containing 1-ethynyl-4-methylbenzene (**A**) moiety exhibited similar luminescence colors in various solvents, the absorption measurement showed negligible changes as the solvent polarity was increased. Similar behavior was also observed for the emission profile. However, 1-ethynyl-4-methylbenzene (**A**) derivatives in dichloromethane and dimethyl sulfoxide showed small red shift. This could presumably be explained as the effect of heavy atoms (chlorine atom in dichloromethane and sulfur atom in dimethyl sulfoxide) of the solvent, which could enhance the triple-state absorption by increasing the intersystem crossing rate (Liu *et al.*, 2001).

Interestingly, 4-ethynyl-*N,N*-dimethylaniline (**B**) derivatives showed identical absorption but exhibited different luminescence colors in each solvent. Differences in emission wavelength of the derivatives in this group suggested that the excited state of 4-ethynyl-*N,N*-dimethylaniline (**B**) derivatives were polarized more

strongly than the ground state.   The more polarized state of the molecules was stabilized by polar solvents, thus resulting in the red-shift of emission wavelength.

Table 5 Absorption wavelength (nm) of 2**A**, 3**A**, 1**B**, 2**B** and 3**B** in various solvents.

Solvents	Compounds				
	2**A**	3**A**	1**B**	2**B**	3**B**
Hexane	319	362			384
ε=1.88	333	382	333	338	405
Ethyl acetate	318	362			
ε=6.02	333	383	341	344	388
Dichloromethane	320	365			390
ε=9.1	336	386	347	349	405
Ethyl alcohol	318	362			
ε=24.55	333	382	339	339	388
Acetonitrile	318	362			
ε=37.5	333	383	344	350	389
Dimethyl sulfoxide	321	368			392
ε=46.7	338	389	353	358	411

Table 6 Emission wavelength (nm) of 2**A**, 3**A**, 1**B**, 2**B** and 3**B** in various solvents.

Solvents	Compounds				
	2**A**	3**A**	1**B**	2**B**	3**B**
Hexane	338	389	371	368	421
ε=1.88	355	408	390	386	442
Ethyl acetate	339	391	433	423	501
ε=6.02	356	411			
Dichloromethane	343	395	437	427	506
ε=9.1	359	415			
Ethyl alcohol	339	391	438	429	514
ε=24.55	356	411			
Acetonitrile	340	393	469	458	555
ε=37.5	355	411			
Dimethyl sulfoxide	345	399	477	464	565
ε=46.7	361	419			

The effect of solvent molecules surrounding the fluorophore in the solution has a significant impact on the differences in energy level between the ground and excited states of fluorophore. These changes cause the molecular dipole moment to be altered and eventually lead to the reorientation of the dipole moment of solvent molecules around the flurophore. In Franck-Condon principle, it states that the time required for the molecule to be excited to a higher energy is much less than that of the rearrangement of the fluorophore and solvent molecules in the solution environment. Therefore, there is a period of delay time between the excitation process and the molecular solvent rearrangement. This results in the increase in dipole moment of the excited state more than that of the ground state as illustrated in figure 25.
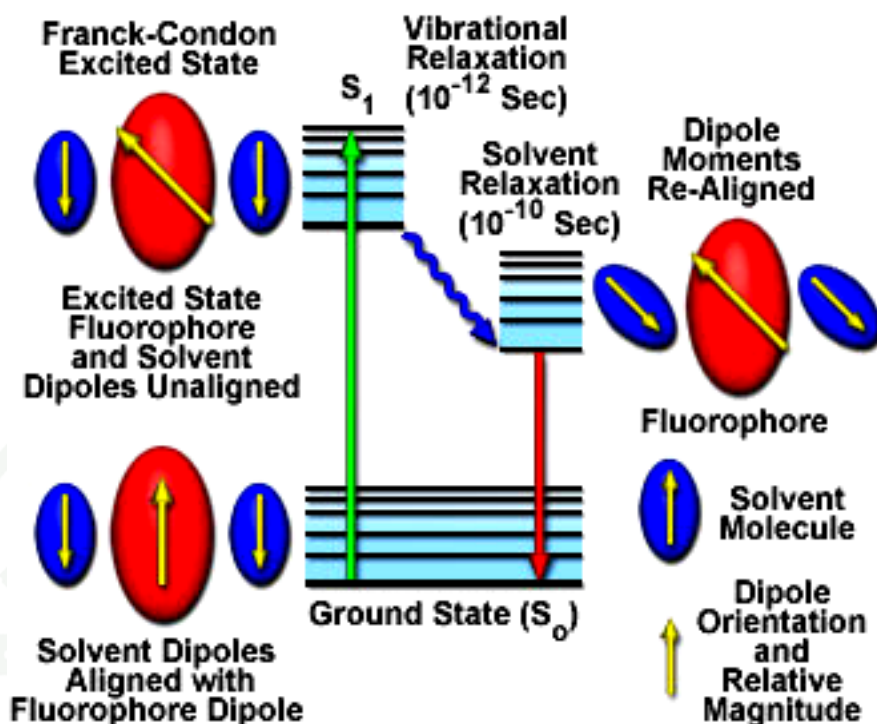
Figure 25 Fluorophore-solvent excited state interaction.

Source: Olympus (2012)

After the flurophore has been excited to higher vibrational states, for example, the first singlet state (S1), the excess of energy will be released to the surrounding environment-the solvent molecules. As a consequence, the fluorophore gradually relaxs to its lowest vibration level in that state, which is normally happens in picoseconds time scale. The solvent molecules that receive the excess amount of energy from the flurophore help stabilize the energy level of the excited state. This process will occur through the reorientation of solvent molecules called the solvent relaxation. In other words, it decreases the energy separation between the ground and the excited states, leading to the red-shift of fluroscence emission. Therefore, if the solvent has high polarity, it will reduce the separation of the energy gap of the excited state and vice versa.

The effect of solvent polarity is one origin of the Stokes shift, which is one of the observations in fluorescence. The Lippert−Mataga equation describes the energy change that results from solvent effects. The Lippert−Mataga equation derivation makes several assumptions. It assumes a spherical fluorophore. It assumes that the dipole vectors for the excited and ground states are similar (this is a reasonable assumption for most fluorophores) (Mihaela *et al.*, 2011). The equations related to the Lippert−Mataga plot are shown;

$$\Delta v = v_{abs} - v_{Flu} = \frac{2(\mu^* - \mu)^2}{4\pi\varepsilon_0 hca^3}\Delta f(\varepsilon, n) + \text{constant}$$

$$\Delta f = \frac{(\varepsilon - 1)}{(2\varepsilon + 1)} - \frac{(n^2 - 1)}{(2n^2 + 1)}$$

where Δv = Stokes shift in cm^{-1}, h = 6.6262 x 10-34 J is Planck's constant, c = 2.99 x 108 m.s^{-1} is the velocity of light, and ε_o = the permittivity of vacuum (8.8542 x 10^{-12} $C^2.N^{-1}.m^{-2}$), *a* is the radius swept out by the fluorophore, μ^* and μ are the excited- and ground-state dipole moments, respectively, and ϵ and *n* are the solvent dielectric constant and refractive index, respectively (Mataga *et al.*, 1956). The Lippert–Mataga plot can be obtained by plotting the Stokes' shift vs. the term in the brackets in the above equation, referred to as the orientation polarizability (Δf) of the solvent, which is the result of both the mobility of the electrons in the solvent and the dipole moment of the solvent.

The solvatochromism data of 1-ethynyl-4-methylbenzene and 4-Ethynyl-*N,N*-dimethylaniline derivatives were analyzed by Lippert-Mataga plot. The 1-ethynyl-4-methylbenzene derivatives showed notable deviation (Figure 26) but the 4-Ethynyl-*N,N*-dimethylaniline derivatives exhibited linear correlations (Figure 27) in the above-mentioned analyses. The Lippert-Mataga equation works fairly well for non-protic solvents because protic solvents, such as water and ethanol, tend to form hydrogen bonds, and result in greater shift than predicted Stokes shifts. However, the effect of the solvent in a Lippert−Mataga plot did not have a clear effect of the
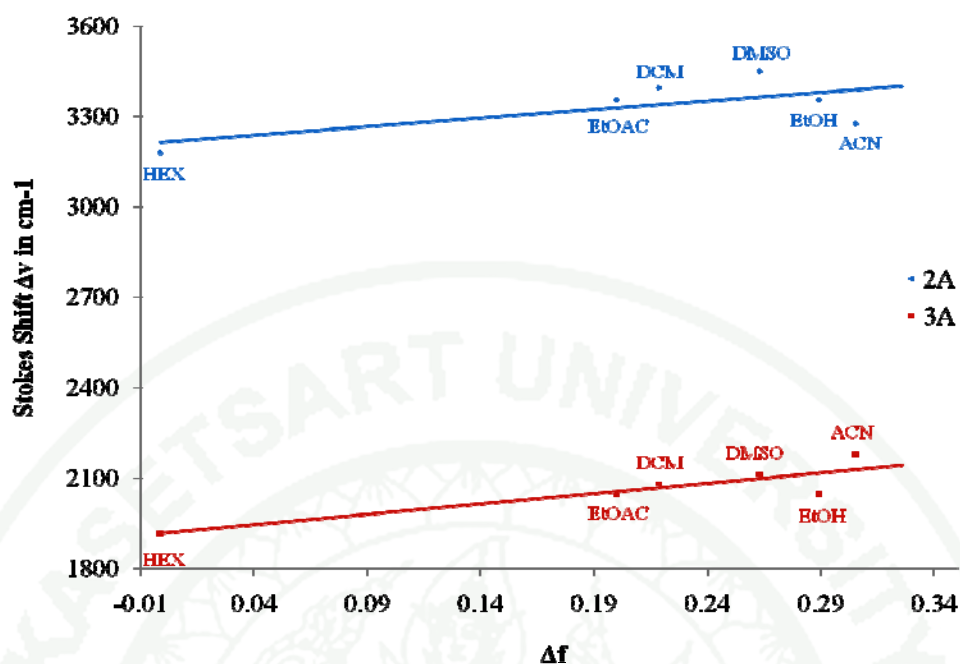
solvent. Therefore, the study of solvent effect should be studied in more detail of other solvents.

Table 7 Stokes shift of 2**A**, 3**A**, 1**B**, 2**B** and 3**B** in various solvents.

Solvents	Parameter		Compounds (nm) [$\Delta v/cm^{-1}$]				
	ϵ	n	2**A**	3**A**	1**B**	2**B**	3**B**
Hexane ε=1.88	1.88	1.3749	36 [3,179]	27 [1,917]	57 [4,389]	30 [2,412]	37 [2,289]
Ethyl acetate ε=6.02	6.02	1.3724	38 [3,357]	29 [2,049]	92 [6,231]	79 [5,429]	113 [5,813]
Dichloromethane ε=9.1	9.1	1.4241	39 [3,395]	30 [2,081]	90 [5,935]	78 [5,234]	116 [5,878]
Ethyl alcohol ε=24.55	24.55	1.3614	38 [3,357]	29 [2,049]	99 [6,667]	90 [6,189]	126 [6,318]
Acetonitrile ε=37.5	37.5	1.3441	37 [3,278]	31 [2,179]	125 [7,748]	108 [6,737]	166 [7,689]
Dimethyl sulfoxide ε=46.7	46.7	1.4793	40 [3,452]	31 [2,111]	124 [7,364]	106 [6,381]	172 [7,746]

Figure 26 Linear plot of Stokes shift verses orientation polarizability (Δ*f*) of 1-ethynyl-4-methylbenzene (**A**) derivatives in various solvents.
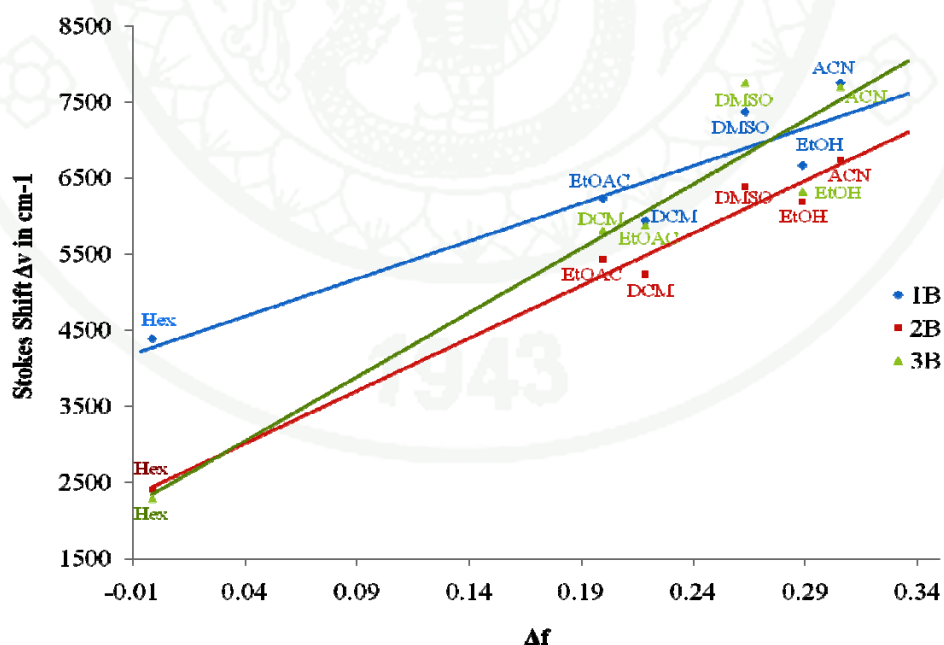

Figure 27 Linear plot of Stokes shift verses orientation polarizability (Δ*f*) of 4-ethynyl-*N*,*N*-dimethylaniline (**B**) functionalized in various solvents.

Theoretical investigations

The absorption energies of all compounds were investigated using the TDDFT method. To obtain more information about the electronic structure of all compounds, theoretical calculation performed with different levels of theory was carried out. The vertical excitation energies in solution were performed using several TD-DFT functional, PBE0 and CAM-B3LYP functional at 6-311G(d,p) level of theory including conductor polarizable continuum model (PCM) solvation based on the optimized structures. The computed vertical excitation energies for singlet excited states, together with the oscillator strength and maximum absorbance calculated using different functionals, compared to experimental results are shown in Figure 28-32.

Theoretical spectra of all compounds were calculated by the linear response (LR) and state-specific (SS) theory. TD-PBE0 and TD-CAM-B3LYP methods in dichloromethane solution are compared with the observed absorption spectra of all compounds in Figures 28-32. TD-CAM-B3LYP performs well than TD-PBE in this system, and therefore, TD-CAM-B3LYP/6-311G(d,p) was used to obtain the energies of the singlet-singlet electronic transitions as well as the oscillator strengths and excitation character of the low-lying excited states. The vertical excitation energies in dichloromethane solution were evaluated within the PCM. The results show that the absorption peaks in dichloromethane solution show red shift compared to those in gas phase of all compound, significantly. The absorption spectra of all compounds were reasonably reproduced by CAM-B3LYP functional in both peak position and intensity. The results shown that the maximum absorbance of all compound using SS-PCM-TD-CAM-B3LYP/6-311G(d,p) methods are in agreement with the experimental results than the other normal LR-PCM-TD-PBE0 and SS-PCM-TD-PBE0 functional.

2A
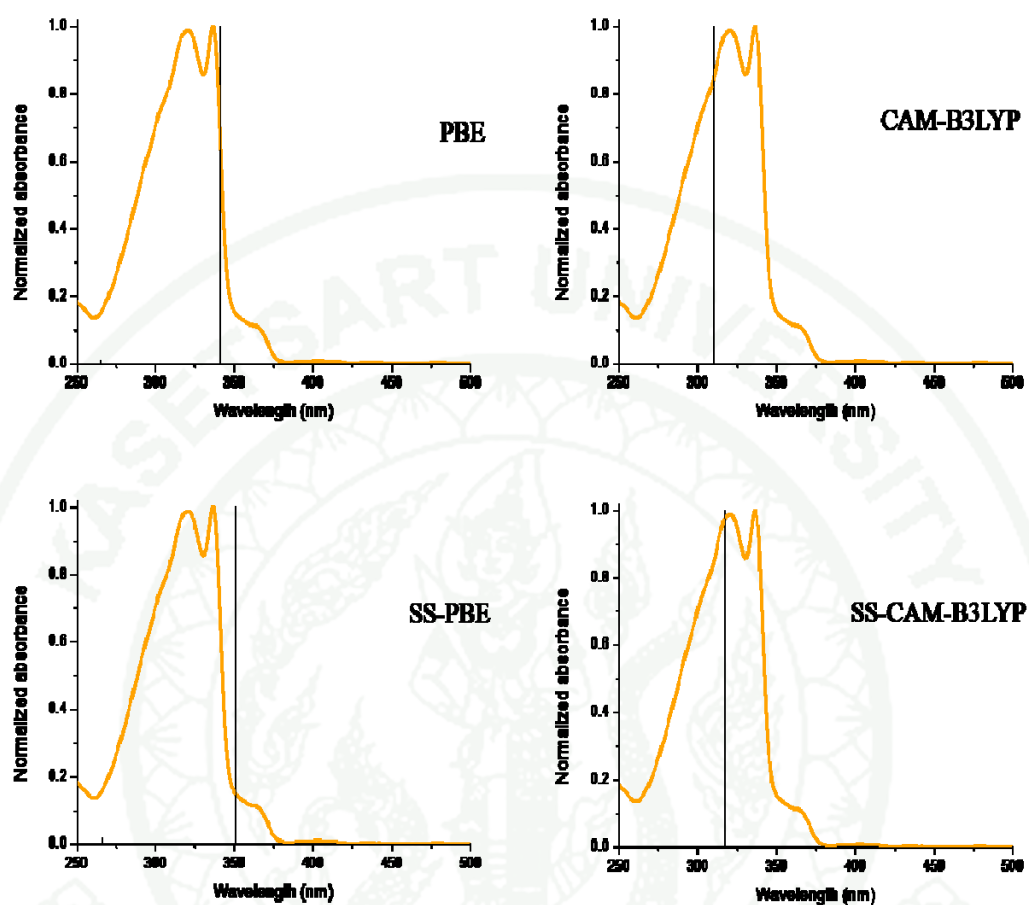
Figure 28 Experimental absorption of 2**A** in dichloromethane solution and
theoretical spectra calculated using PBE0, CAM-B3LYP, SS-PBE0 and
SS-CAM-B3LYP in dichloromethane.

3A
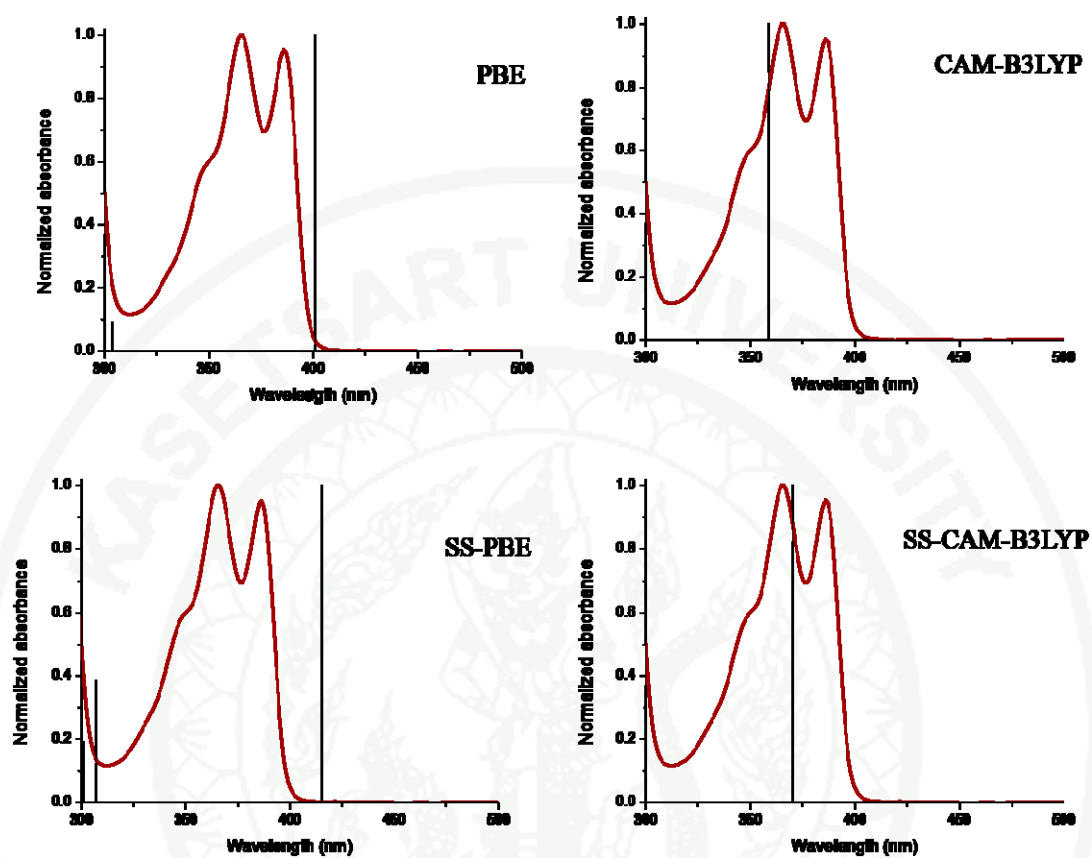
Figure 29 Experimental absorption of 3**A** in dichloromethane solution and
theoretical spectra calculated using PBE0, CAM-B3LYP, SS-PBE0 and
SS-CAM-B3LYP in dichloromethane.

1B

Figure 30 Experimental absorption of 1**B** in dichloromethane solution and
theoretical spectra calculated using PBE0, CAM-B3LYP, SS-PBE0 and
SS-CAM-B3LYP in dichloromethane.

2B

Figure 31 Experimental absorption of 2**B** in dichloromethane solution and
theoretical spectra calculated using PBE0, CAM-B3LYP, SS-PBE0 and
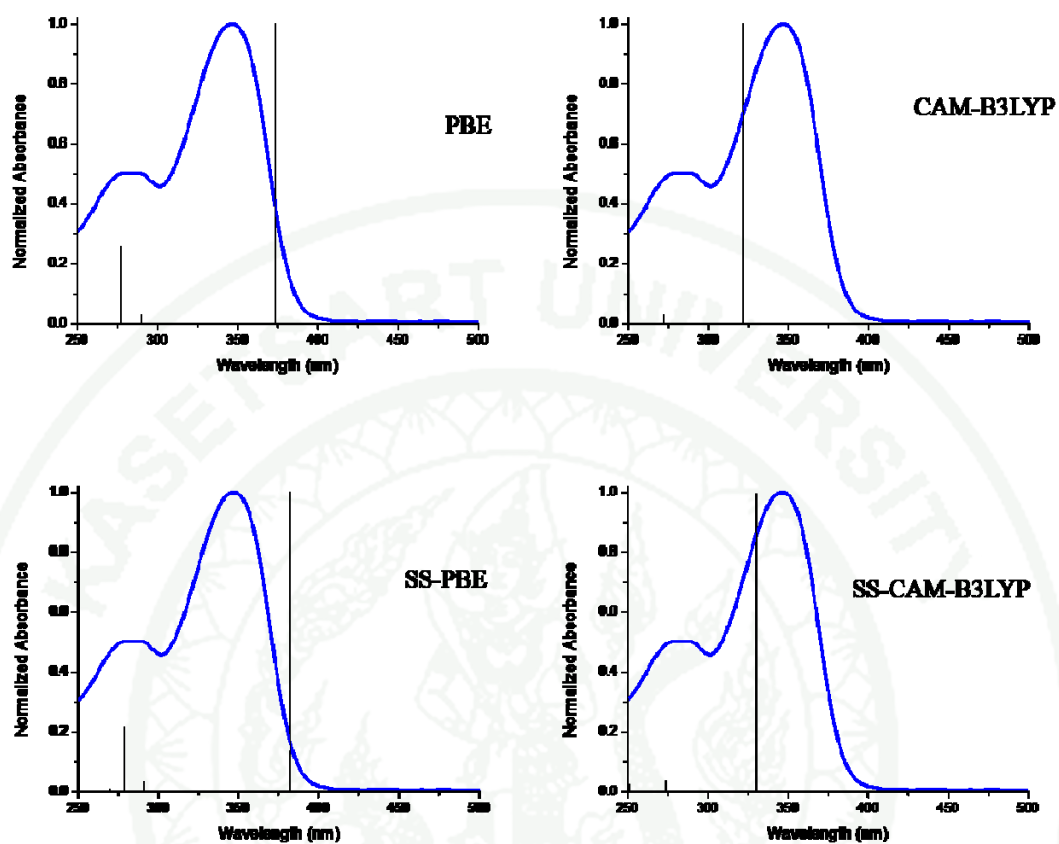SS-CAM-B3LYP in dichloromethane.

3B

Figure 32 Experimental absorption of 3**B** in dichloromethane solution and
theoretical spectra calculated using PBE0, CAM-B3LYP, SS-PBE0 and
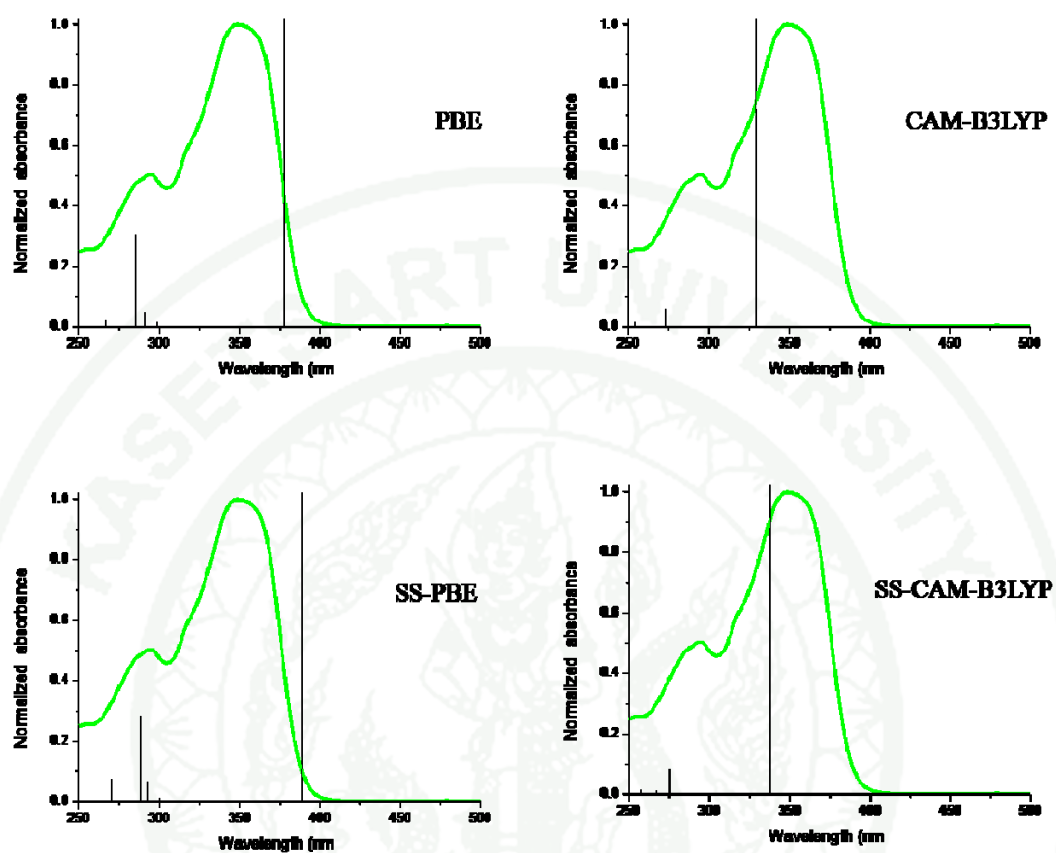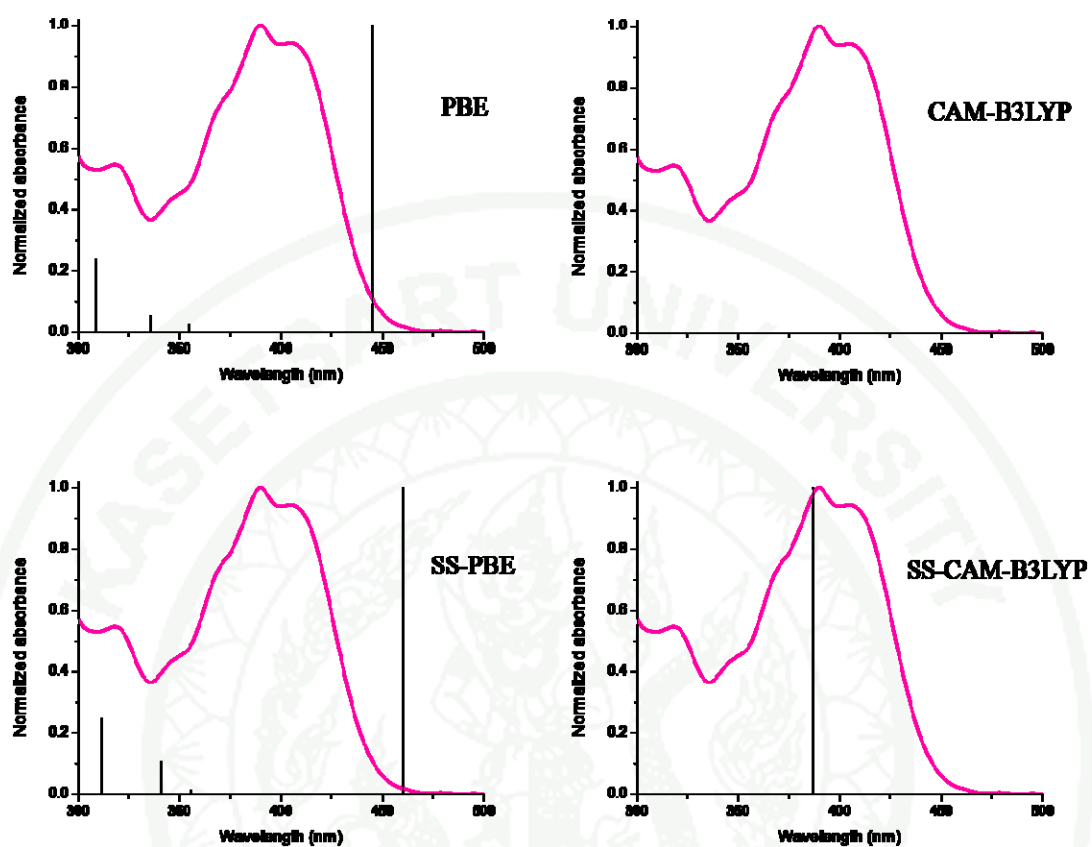SS-CAM-B3LYP in dichloromethane.

Table 8 Experimental absorption energy (λ^{ex}_{max} (nm)) of compounds in
dichloromethane solution compared with theoretical result calculated using
PBE0, and SS-PBE0 in dichloromethane

Compounds	TD-PBE0	$\Delta\lambda$	SS-TD-PBE0	$\Delta\lambda$	Expt.
1**A**	330	-	339	-	-
2**A**	341	21	351	31	320,336
3**A**	401	36	415	50	365,386
1**B**	373	26	383	36	347
2**B**	378	29	389	40	349
3**B**	445	55	460	70	390,405

Table 9 Experimental absorption energy (λ^{ex}_{max} (nm)) of compounds in
dichloromethane solution compared with theoretical result calculated using
CAM-B3LYP, and SS-CAM-B3LYP in dichloromethane

Compounds	TD-CAM-B3LYP	$\Delta\lambda$	SS-TD-CAM-B3LYP	$\Delta\lambda$	Expt.
1**A**	299	-	306	-	-
2**A**	310	10	317	3	320,336
3**A**	359	6	370	5	365,386
1**B**	322	25	330	17	347
2**B**	329	20	337	12	349
3**B**	376	14	387	3	390,405

In Table 8-9, we focus on the TD-DFT absorption wavelengths of the 1-ethynyl-4-methylbenzene and 4-Ethynyl-*N*,*N*-dimethylaniline derivatives in gas phase and in dichloromethane solution compared with the experimental absorption spectra shown in Tables 4. For 1-ethynyl-4-methylbenzene and 4-Ethynyl-*N*,*N*-dimethylaniline derivatives, the deviations from the experimental values in peak position were overestimated within about 20-70 nm in both of gas phase and in solution for TD-PBE0 calculations. Conversely, TD-CAM-B3LYP calculations, the deviations from the experimental values in peak position were with about 30 and 15 nm both in gas phase and in solution, respectively, which is partly attributed to the solvent effect and/or our model neglecting the side chain. Therefore, the excitation energies in solution are in better agreement with the experimental data. CAM-B3LYP functional, an improved hybrid functional with long-range correction, performs well for the excited states of large π-conjugated system. The results show that SS-PCM0-TD-CAM-B3LYP provides the better results than those of TD-PBE0. Therefore, we present the assignments and interpretation of the absorption spectra based on the SS-PCM-TD-CAM-B3LYP results.

Next, we discuss the transition probabilities of 1-ethynyl-4-methylbenzene and 4-Ethynyl-*N*,*N*-dimethylaniline derivatives. The shape of absorption spectra or the peak with largest transition probabilities of 4-Ethynyl-*N*,*N*-dimethylaniline derivatives are similar to those of 1-ethynyl-4-functionalized. 1-ethynyl-4-methylbenzene and 4-Ethynyl-*N*,*N*-dimethylaniline derivatives have the first peak corresponding to the electronic excitation from HOMO to LUMO (H→L) and the second peak from next HOMO (HOMO-1) to LUMO (H-1→L) transition. This feature was interpreted by the variation of the molecular orbitals due to the different substituted groups. The molecular orbitals relevant for the low-lying excited states molecular are given in Figures 33-35.

1A

HOMO   LUMO

(a)

1B

HOMO   LUMO

(b)
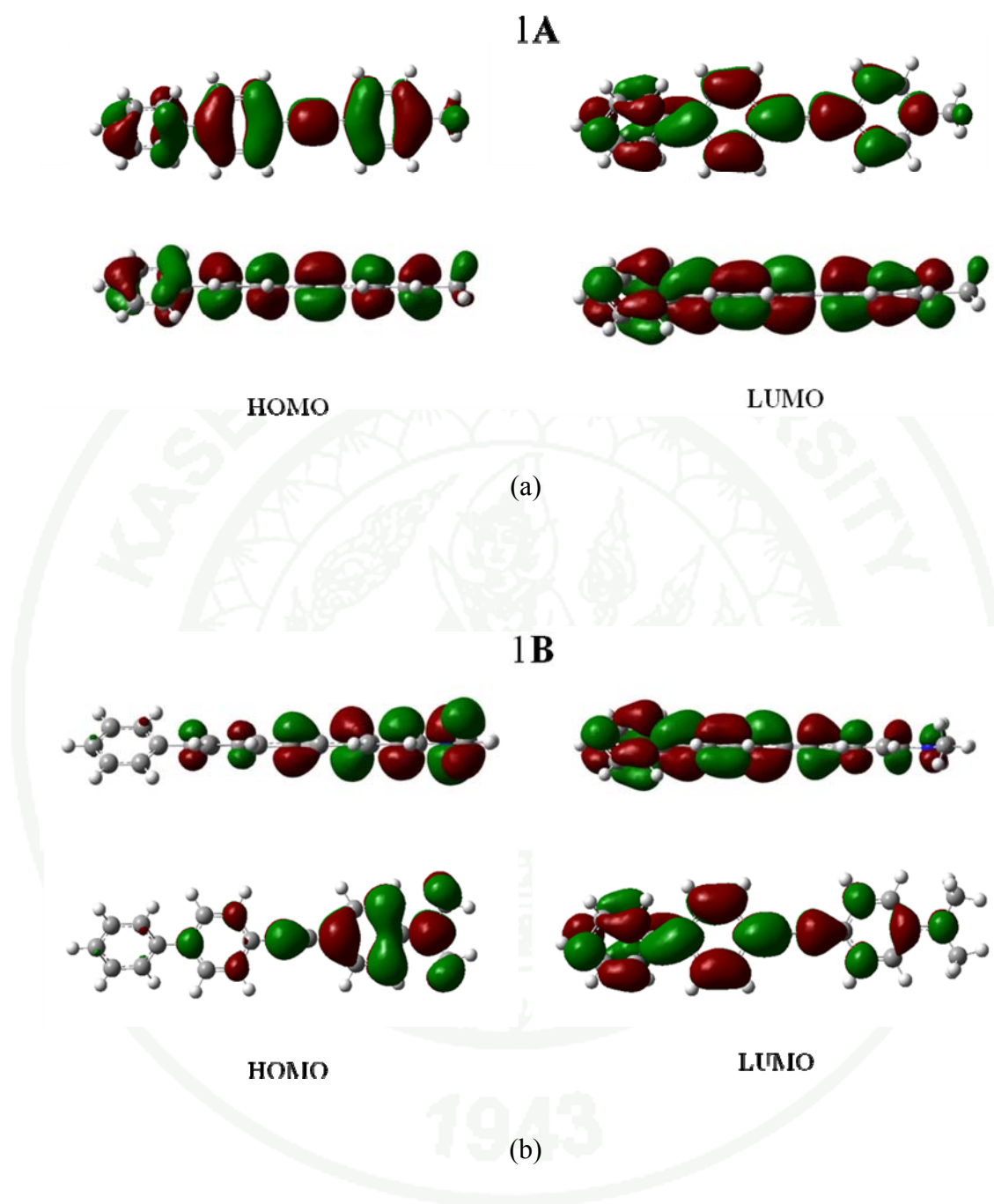
Figure 33 Molecular orbitas isosurface plots of frontier molecular orbital (HOMO
and LUMO) for the (a) 1**A** and (b) 1**B** compounds.

2A

HOMO   LUMO

(a)

2B

HOMO   LUMO

(b)
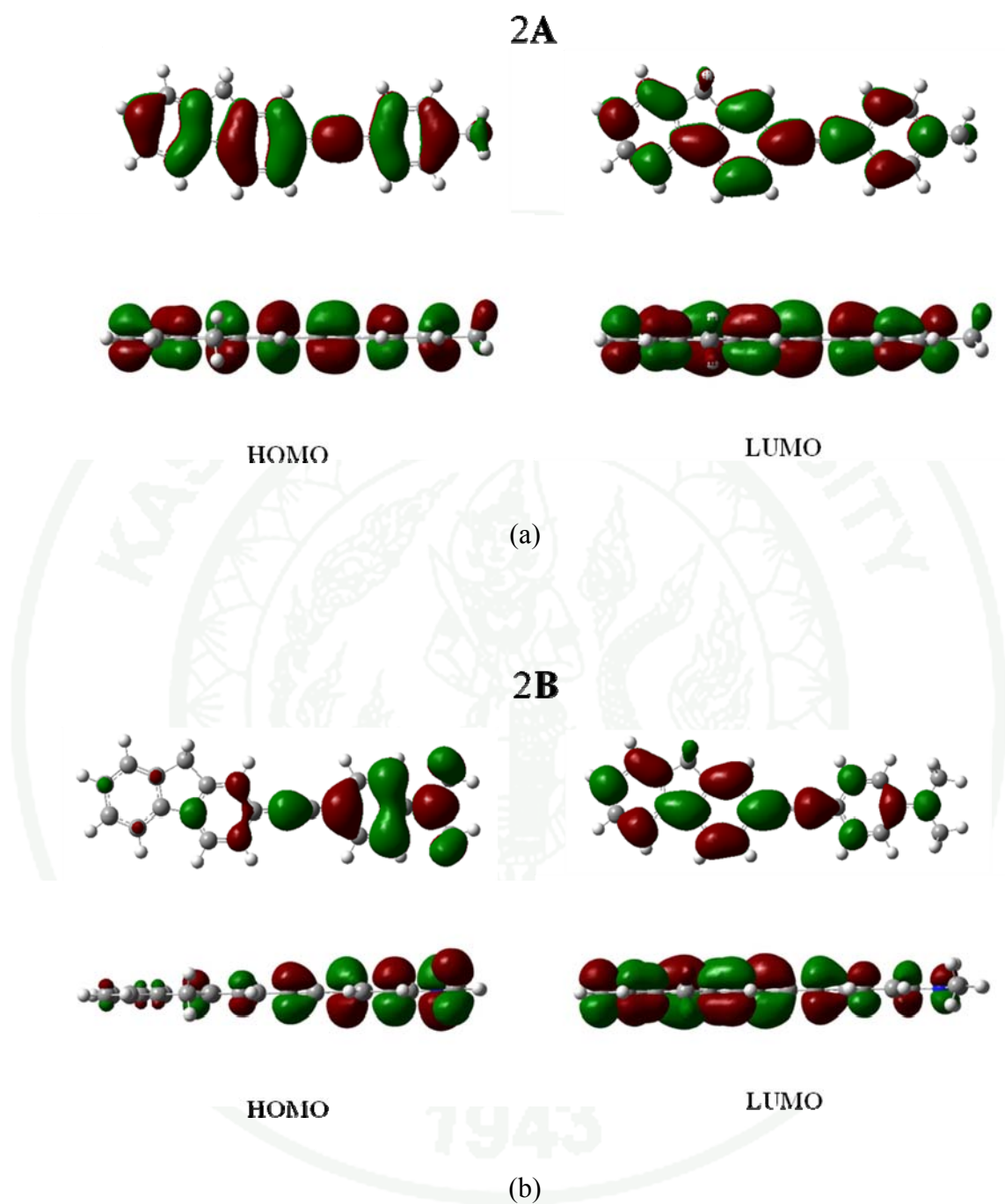
Figure 34 Molecular orbitas isosurface plots of frontier molecular orbital (HOMO
and LUMO) for the (a) 2**A** and (b) 2**B** compounds.

3A

HOMO   LUMO

(a)

3B

HOMO   LUMO

(b)
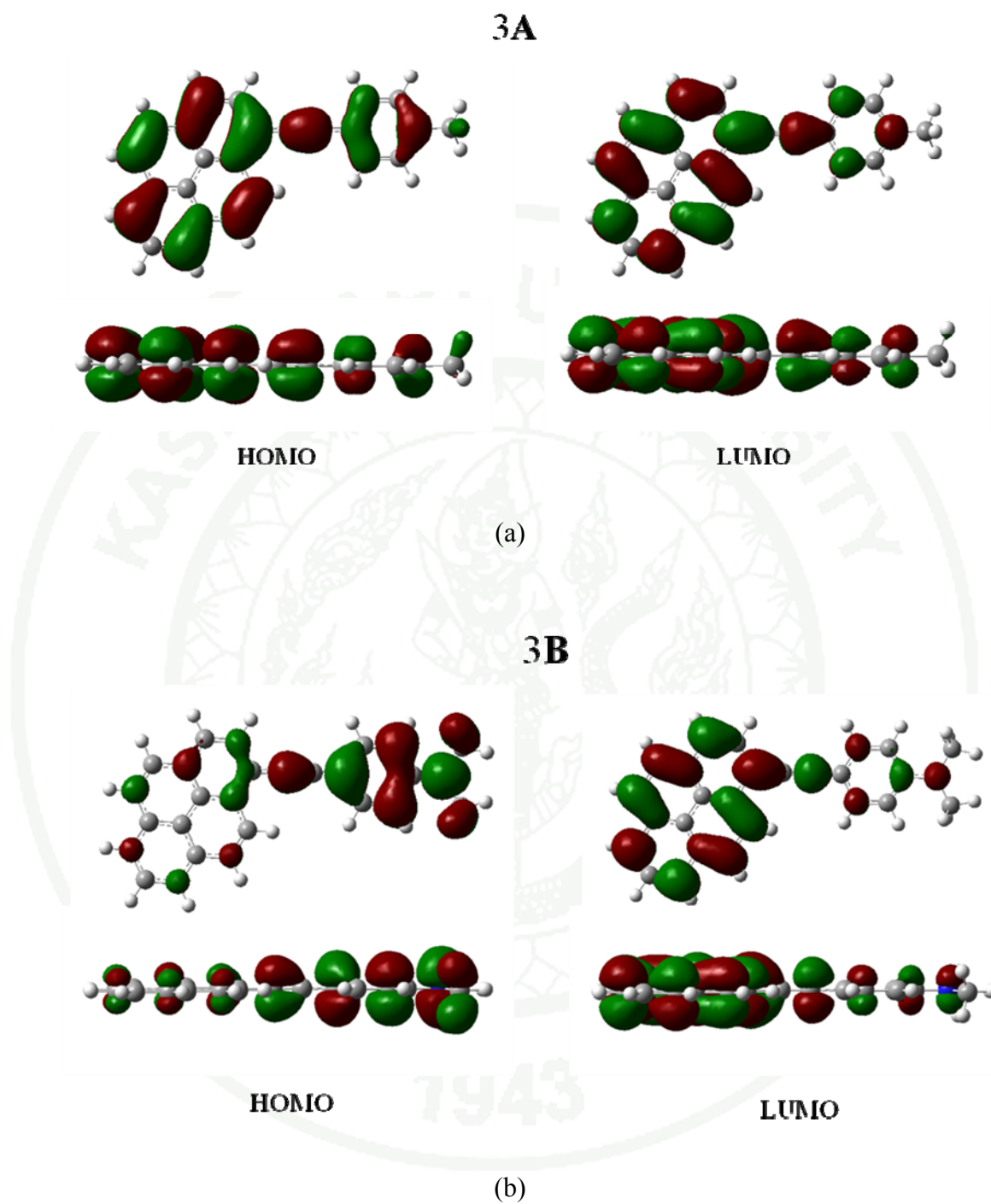
Figure 35 Molecular orbitas isosurface plots of frontier molecular orbital (HOMO and LUMO) for the (a) 3**A** and (b) 3**B** compounds.

The frontier orbital appearances of the prepared compounds calculated by CAM-B3LYP level of theory were shown in Figure 33-35. The whole parts of the compounds containing 1-ethynyl-4-methylbenzene group were concerned with their characteristics of both HOMOs and LUMOs. The shape of HOMOs and LUMOs illustrated that HOMOs and LUMOs were π and π^* orbitals, respectively. On the other hand, in the compounds with amine group, the 4-Ethynyl-*N,N*-dimethylaniline part involved in the structure of HOMOs but the aromatic nucleus contributed to the structures of LUMOs. The results indicated the HOMOs were likely to be the n orbitals corresponding to the electron donor part of amine group and the LUMOs were inclined to be the π^* of the aromatic nuclei. By using pictorial approach, the transition from HOMO to LUMO of the compounds with the 1-ethynyl-4-methylbenzene group was the transition from π to π^*. However, the transition from HOMO to LUMO of the compounds with the 4-Ethynyl-*N,N*-dimethylaniline group was the n to π^* transition which had the smaller energy gap than the transition from π to π^*. This was the reason of the trend of absorption wavelengths that observed in the experimental section.

CONCULSION

1-ethynyl-4-methylbenzene and 4-Ethynyl-*N,N*-dimethylaniline derivatives could be synthesized using microwave-assisted, palladium-catalyzed Sonogashira-type coupling reaction. The products were characterized by ^1H-NMR, FT-IR, UV-Vis and fluorescence measurements. Analysis of the absorption and emission behaviors indicated that the extended conjugation resulting from the substituent can further red shifts in the absorption and emission spectra. The experimental data agreed well with the results obtained from quantum chemical calculations. It can serve as new luminescence materials for fabricating OLED-based full-color displays.

LITERATURE CITED

Angel, U.N. 2008. **The basics of organic light emitting diodes.** Available Source: http://lcp.elis.ugent.be/tutorials/tut_oled#what, December 22, 2010.

Baathulaa, K., Y. Xu and X. Qian. 2010. Unusual large Stokes shift and solvatochromic fluorophore: Synthesis, spectra, and solvent effect of 6-substituted 2,3-naphthalimide. **J. Photochem. Photobiol. A** 216(1):24-34.

Borrett, A. 2010. **The next generation of LCDs.** Available Source: http://www2.hull.ac.uk/researchandinnovation/creativeeconomy/thenextgeneration.aspx, December 21, 2010.

Brase, S., J.H. Kirchhoffb and J. Ko¨bberling. 2002. Palladium-catalysed reactions in solid phase organic synthesis. **Tetrahedron** 59885–939.

Brunner, K., A. van Dijken, H. Börner, J.J.A.M. Bastiaansen, N.M.M. Kiggen and B.M.W. Langeveld. 2004. Carbazole Compounds as Host Materials for Triplet Emitters in Organic Light-Emitting Diodes: Tuning the HOMO Level without Influencing the Triplet Energy in Small Molecules. **J. Am. Chem. Soc.** 126(19):6035-6042.

Changdev, N.R., B.M. Ramchandra, M.B. Sandeep, A.J. Ravindra and P.M. Pramod. 2009. Microwave-assisted Sonogashira coupling of novel 2-[6-(arylethynyl)pyridin-3-yl]-1H-benzimidazole derivatives. **ARKIVOC** 2009(9):105-114.

Erdélyi, M. and A. Gogoll. 2001. Rapid Homogeneous-Phase Sonogashira Coupling Reactions Using Controlled Microwave Heating. **J. Org. Chem.** 66(12):4165-4169.

Esward, T.J. and V.P. Sokhan. 2006. Mathematical Modelling for Metrology at the Nanoscale. **NPL Report DEM-ES 005**

Fleischmann, M. 2007. **OLED Coming This Year.** Available Source: http://www.hometheater.com/news/041307oled/, December 14, 2010.

Gerakines, P.A., W.A. Schutte, J.M. Greenberg and E.F.v. Dishoeck. 1995. The infrared band strengths of H_2O, CO and CO_2 in laboratory simulations of astrophysical ice mixtures. **Astronomy & Astrophysics.** 296810.

Gigante, B., M.A. Esteves, N. Pires, M.L. Davies, P. Douglas, S.M. Fonseca, H.D. Burrows, R.A.E. Castro, J. Pina and J. Seixas de Melo. 2009. Synthesis, spectroscopy, photophysics and thermal behaviour of stilbene-based triarylamines with dehydroabietic acid methyl ester moieties. **New J. Chem.** 33(4):877-885.

Hancock, J.M., A.P. Gifford, Y. Zhu, Y. Lou and S.A. Jenekhe. 2006. n-Type Conjugated Oligoquinoline and Oligoquinoxaline with Triphenylamine Endgroups: Efficient Ambipolar Light Emitters for Device Applications. **Chem. Mater.** 18(20):4924-4932.

Hinsen, K. 2000. The molecular modeling toolkit: A new approach to molecular simulations. **J. Comput. Chem.** 21(2):79-85.

Ho, T.-I., A. Elangovan, H.-Y. Hsu and S.-W. Yang. 2005. Highly Fluorescent N,N-Dimethylaminophenylethynylarenes: Synthesis, Photophysical Properties, and Electrochemiluminescence. **J. Phys. Chem. B** 109(18):8626-8633.

Holmes, R.J., S.R. Forrest, Y.J. Tung, R.C. Kwong, J.J. Brown, S. Garon and M.E. Thompson. 2003. Blue organic electrophosphorescence using exothermic host–guest energy transfer. **Appl. Phys. Lett.** 82(15):2422.

Jim, C. 2007. **UV-Visible absorption spectra.** Available Source: http://www.chemguide.co.uk/analysis/uvvisible/theory.html, September 20, 2012.

John, C. 2000. Interpretation of Infrared Spectra, A Practical Approach John. Wiley & Sons Ltd, Chichester

Kapoor, N. and K.R.J. Thomas. 2010. Fluoranthene-based triarylamines as hole-transporting and emitting materials for efficient electroluminescent devices. **New J. Chem.** 34(12):2739-2748.

Kordas, J. and M.A. El-Bayoumi. 1974. Excited state intramolecular torsional relaxation. Viscosity, temperature, and medium effects on the fluorescence characteristics of a sterically crowded molecule. **J. Chem. Soc.** 96(10):3043-3048.

Larhed, M. and A. Hallberg. 1996. Microwave-Promoted Palladium-Catalyzed Coupling Reactions. **J. Org. Chem.** 61(26):9582-9584.

Lee, M.-T., C.-K. Yen, W.-P. Yang, H.-H. Chen, C.-H. Liao, C.-H. Tsai and C.H. Chen. 2004. Efficient Green Coumarin Dopants for Organic Light-Emitting Devices. **Org. Lett.** 6(8):1241-1244.

Liao, L.S., K.P. Klubek and C.W. Tang. 2004. High-efficiency tandem organic light-emitting diodes. **Appl. Phys. Lett.** 84(2):167.

Liu, C., X. Wang, Q. Gong, Y. Liu, W. Qiu and D. Zhu. 2001. External heavy atom effect on optical limiting performance of conjugated phthalocyanine pentamer. **Chem. Phys. Lett.** 347(4–6):378-382.

Liu, F., W.-Y. Lai, C. Tang, H.-B. Wu, Q.-Q. Chen, B. Peng, W. Wei, W. Huang and Y. Cao. 2008. Synthesis and Characterization of Pyrene-Centered Starburst Oligofluorenes. **Macromol. Rapid Commun.** 29(8):659-664.

Mataga, N., Y. Kaifu and M. Koizumi. 1956. Solvent Effects upon Fluorescence Spectra and the Dipolemoments of Excited Molecules. **Bull. Chem. Soc. Jpn.** 29(4):465-470.

Mihaela, H., A. Airinei and D.O. Dorohoi. 2011. Solvent effects on the electronic absorption and fluorescence spectra. **J. Adv. Res. Phys.** 2(1):011105.

Morgado, J., N. Barbagallo, A. Charas, M. Matos, L. Alcácer and F. Cacialli. 2003. Self-assembly surface modified indium–tin oxide anodes for single-layer light-emitting diodes. **J. Phys. D: Appl. Phys.** 36(5):434.

Nantalaksakul, A., A. Mueller, A. Klaikherd, C.J. Bardeen and S. Thayumanavan. 2009. Dendritic and Linear Macromolecular Architectures for Photovoltaics: A Photoinduced Charge Transfer Investig ation. **J. Am. Chem. Soc.** 131(7):2727-2738.

Olympus. 2012. **Fluorophore-solvent excited state interaction.** Available Source: http://www.olympusmicro.com/primer/java/jablonski/solventeffects/index.html, September 20, 2012.

Park, J.-W., P. Kang, H. Park, H.-Y. Oh, J.-H. Yang, Y.-H. Kim and S.-K. Kwon. 2010. Synthesis and properties of blue-light-emitting anthracene derivative with diphenylamino-fluorene. **Dyes Pigm.** 85(3):93-98.

Pu, Y.-J., A. Kamiya, K.-i. Nakayama and J. Kido. 2010. Arylamino-9,10-diphenylanthracenes for organic light emitting devices. **Organic Electronics** 11(3):479-485.

Scalmani, G. and M.J. Frisch. 2010. Continuous surface charge polarizable continuum models of solvation. I. General formalism. **J. Chem. Phys**. 132(11):114110-114115.

Shirota, Y. and H. Kageyama. 2007. Charge Carrier Transporting Molecular Materials and Their Applications in Devices. **Chem. Rev.** 107(4):953-1010.

Shtein, M., P. Peumans, J.B. Benziger and S.R. Forrest. 2004. Direct, Mask- and Solvent-Free Printing of Molecular Organic Semiconductors. **Adv. Mater.** 16(18):1615-1620.

Sonar, P., M.S. Soh, Y.H. Cheng, J.T. Henssler and A. Sellinger. 2010. 1,3,6,8-Tetrasubstituted Pyrenes: Solution-Processable Materials for Application in Organic Electronics. **Org. Lett.** 12(15):3292-3295.

Suramitr, S., W. Meeto, P. Wolschann and S. Hannongbua. 2010. Understanding on absorption and fluorescence electronic transitions of carbazole-based conducting polymers: TD-DFT approaches. **Theor. Chem. Acc.** 125(1):35-44.

Suramitr, S., S. Phalinyot, P. Wolschann, R. Fukuda, M. Ehara and S. Hannongbua. 2011. Photophysical Properties and Photochemistry of EE-, EZ-, and ZZ-1,4-Dimethoxy-2,5-bis[2-(thien-2-yl)ethenyl] Benzene in Solution: Theory and Experiment. **J. Phys. Chem. A** 116(3):924-937.

Thomas, K.R., N. Kapoor, M.N. Bolisetty, J.H. Jou, Y.L. Chen and Y.C. Jou. 2012. Pyrene-fluorene hybrids containing acetylene linkage as color-tunable emitting materials for organic light-emitting diodes. **J. Org. Chem.** 77(8):3921-3932.

Tomasi, J., B. Mennucci and R. Cammi. 2005. Quantum Mechanical Continuum Solvation Models. **Chem. Rev.** 105(8):2999-3094.

Wei, M.K., C.W. Lin, C.C. Yang, Y.W. Kiang, J.H. Lee and H.Y. Lin. 2010. Emission characteristics of organic light-emitting diodes and organic thin-films with planar and corrugated structures. **Int. J. Mol. Sci.** 11(4):1527-1545.

Yanai, T., D.P. Tew and N.C. Handy. 2004. **Chem. Phys. Lett**. 39351.

Yang, J., A. Dass, A.-M.M. Rawashdeh, C. Sotiriou-Leventis, M.J. Panzner, D.S. Tyson, J.D. Kinder and N. Leventis. 2004. Arylethynyl Substituted 9,10-Anthraquinones: Tunable Stokes Shifts by Substitution and Solvent Polarity. **Chem. Mat.** 16(18):3457-3468.

Yu, Y.-H., C.-H. Huang, J.-M. Yeh and P.-T. Huang. 2011. Effect of methyl substituents on the N-diaryl rings of anthracene-9,10-diamine derivatives for OLEDs applications. **Organic Electronics** 12(4):694-702.

Zakerhamidi M. S, G. A and M. M. 2012. Solvent Effects on the UV/ Visible Absorption Spectra of Some Aminoazobenzene. **Dyes. Chem. Sci. Trans.** 1(1):1-8.
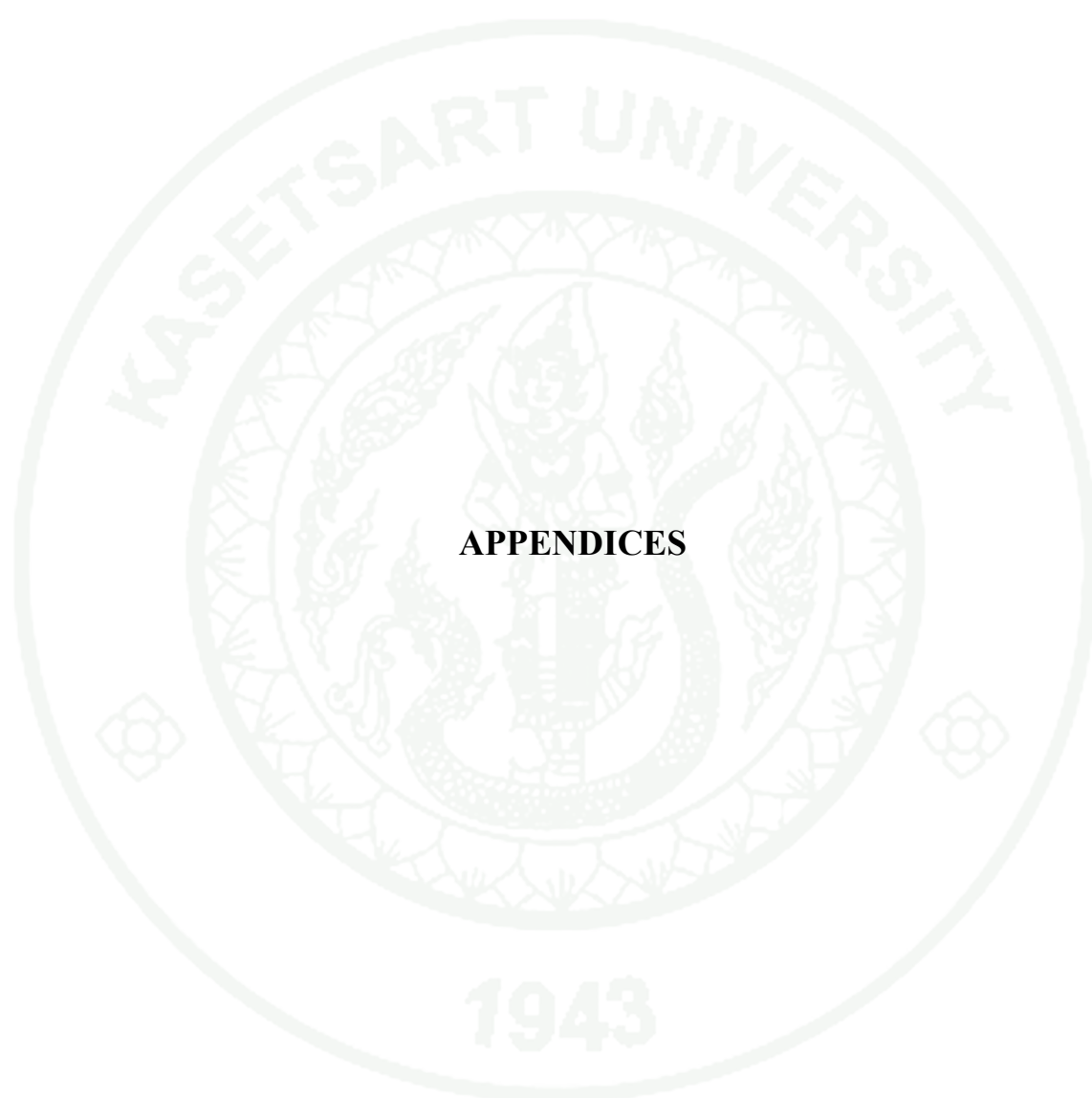
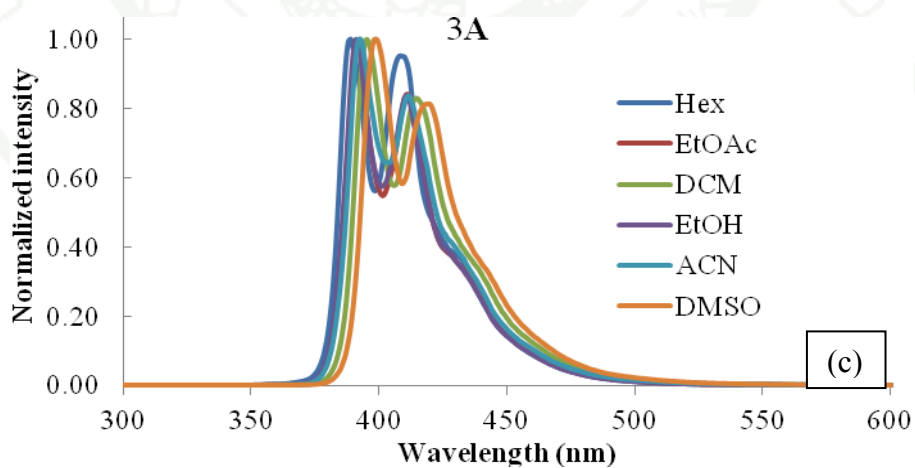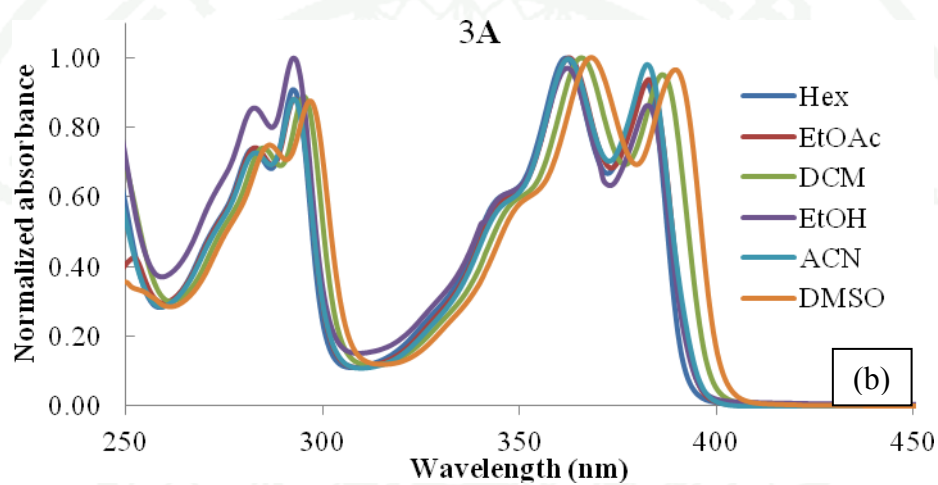**APPENDICES**
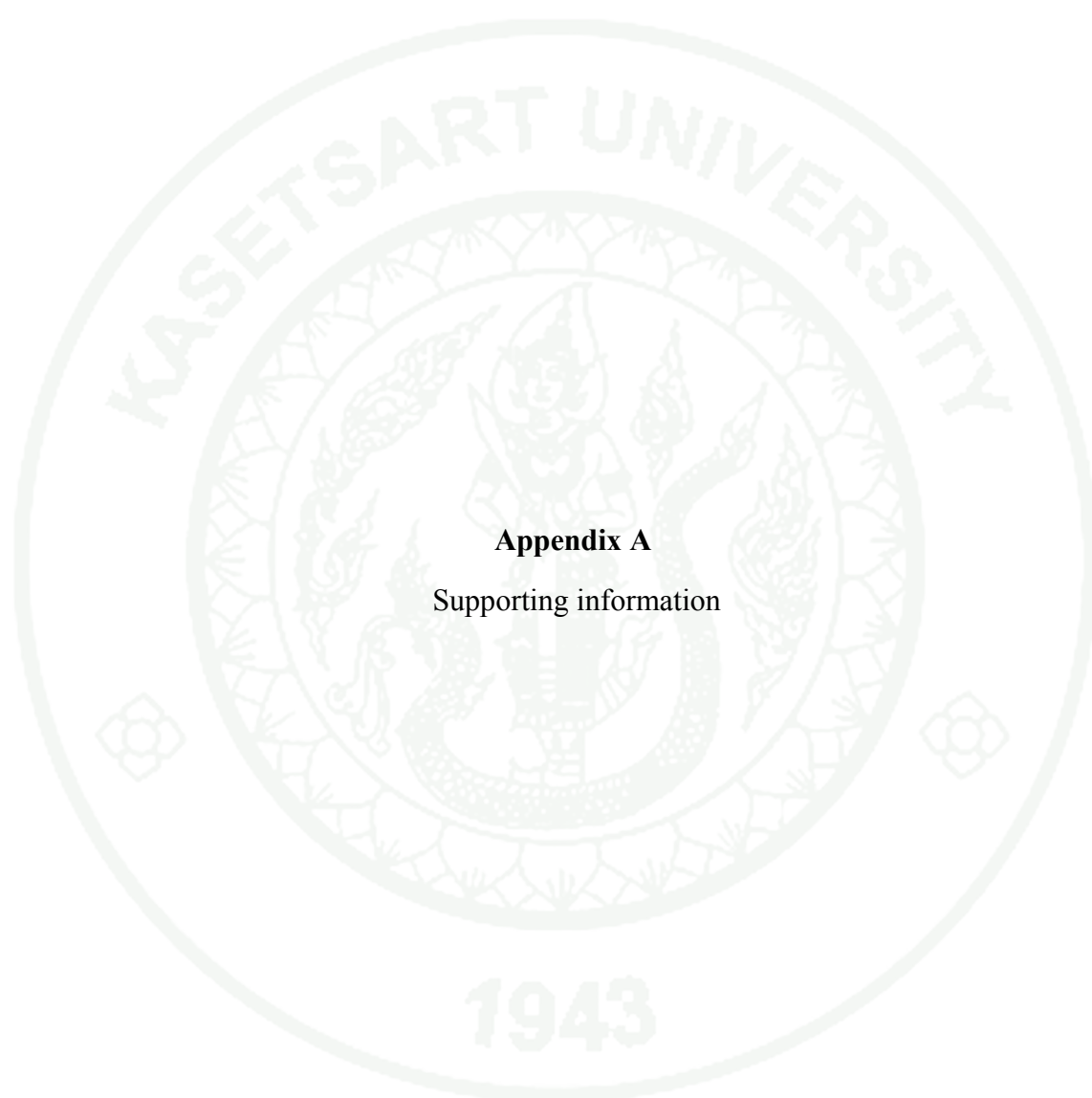
Appendix A

Supporting information
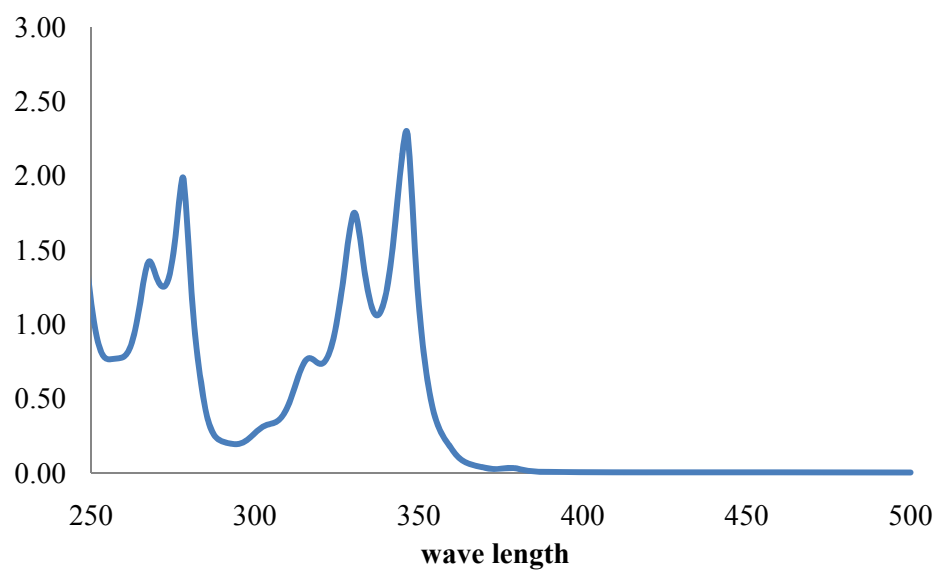
Appendix Figure A1 UV-vis spectra of 1-bromopyrene in dichloromethane.
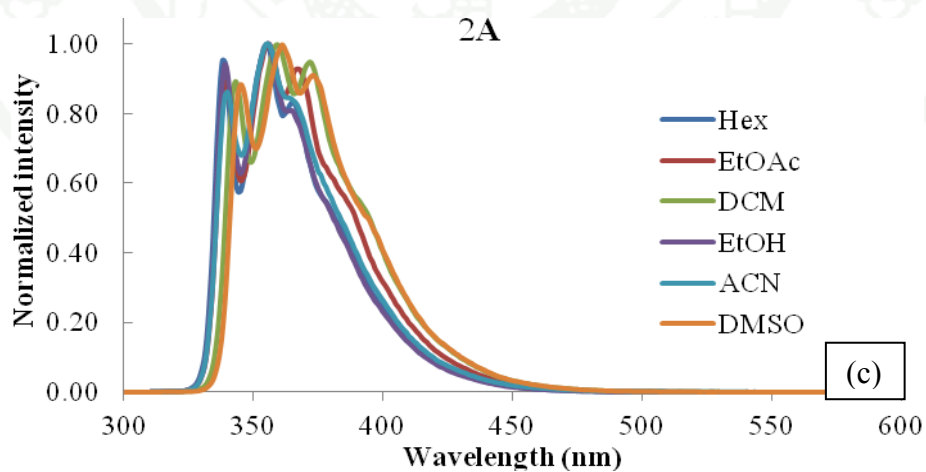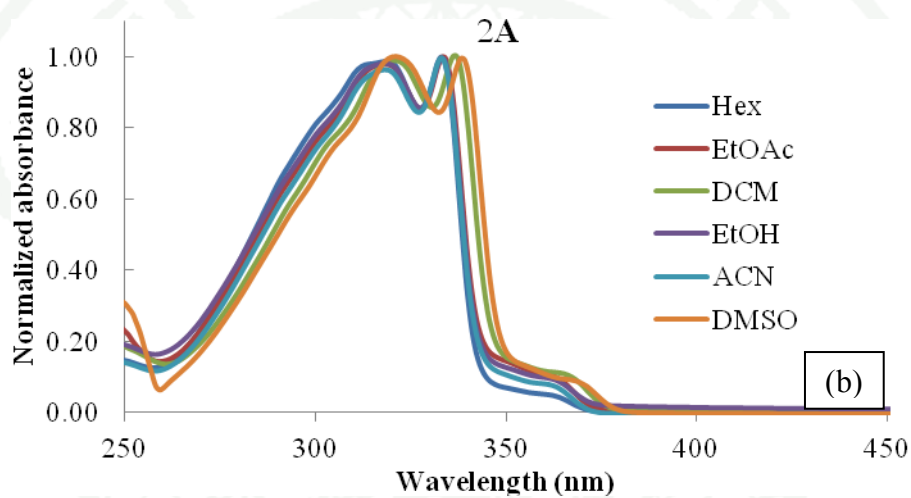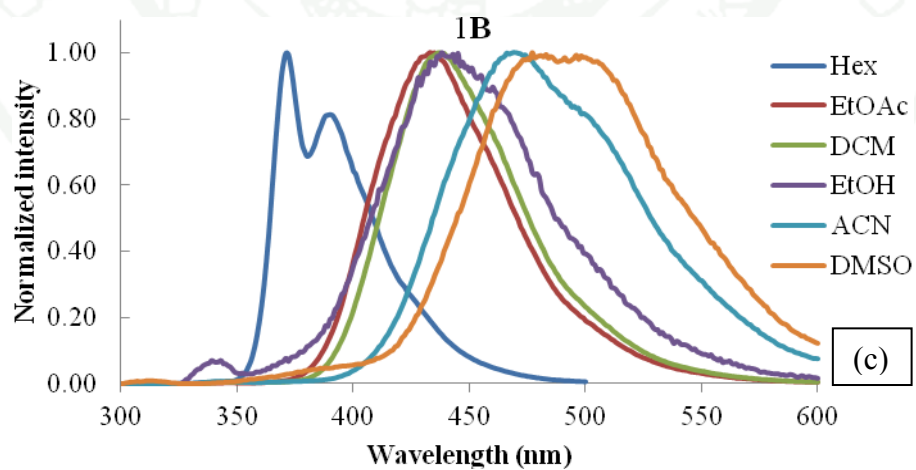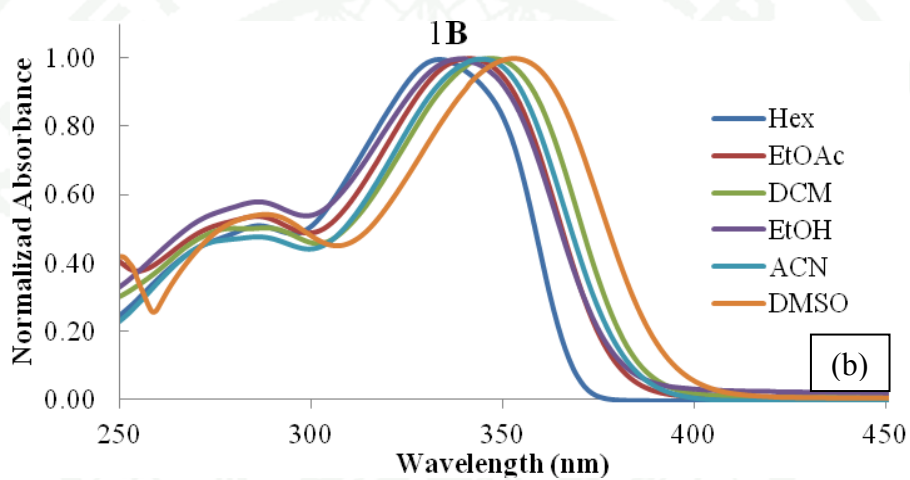
Appendix Figure A2 (a) Optical image, (b) absorption and (c) emission spectra of
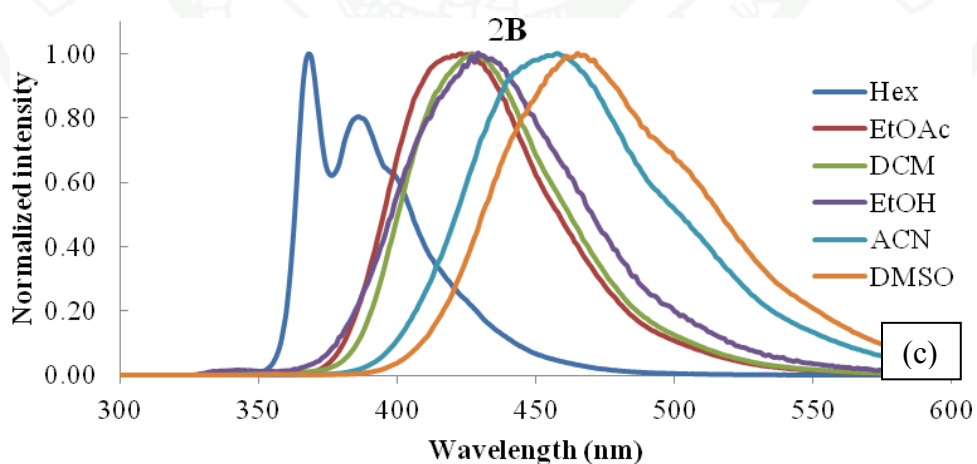4-((4aH-fluoren-7-yl)ethynyl)-methylbenzene 2**A** in the
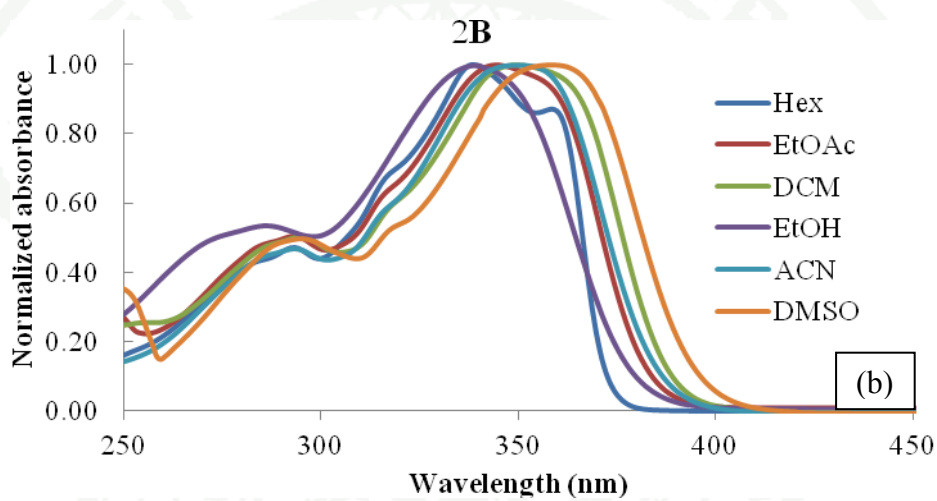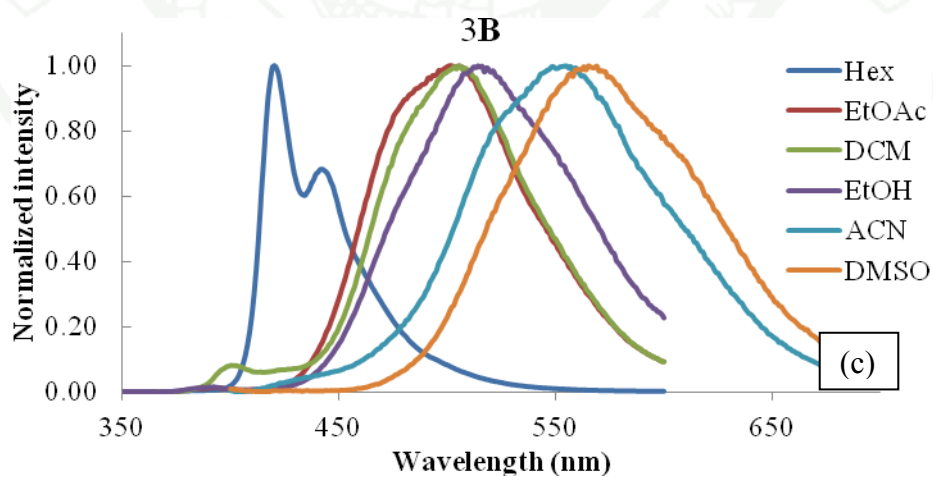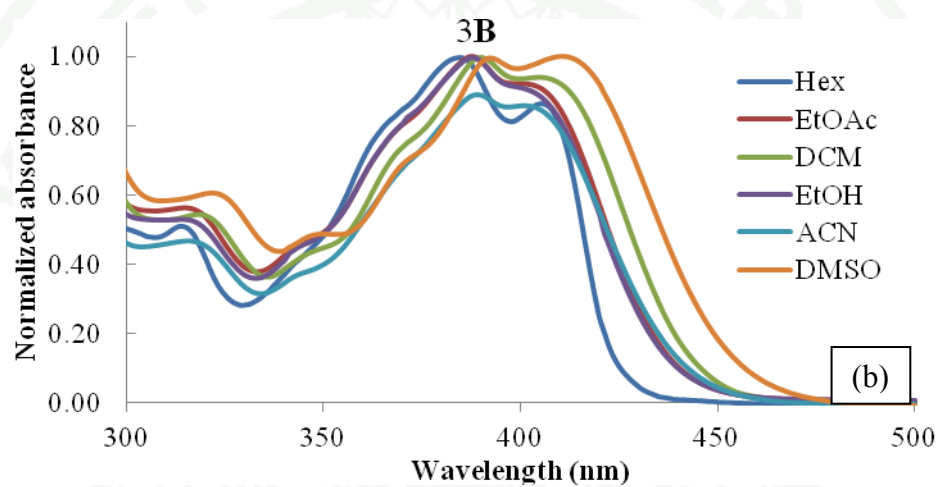various solvents.

Appendix Figure A3 (a) Optical image, (b) absorption and (c) emission spectra of
4-(pyren-1-ylethynyl)-methylbenzene (3**A**) in the various
solvents.

Appendix Figure A4 (a) Optical image, (b) absorption and (c) emission spectra of
4-(biphenyl-4-ylethynyl)-*N,N*-dimethylaniline (1**B**) in the
various solvents.

Appendix Figure A5 (a) Optical image, (b) absorption and (c) emission spectra of
4-((4aH-fluoren-7-yl)ethynyl)-*N,N*-dimethylaniline (2**B**)
in the various solvents.

Appendix Figure A6 (a) Optical image, (b) absorption and (c) emission spectra of 4-(pyren-1-ylethynyl)-*N,N*-dimethylaniline (3**B**) in the various solvents.
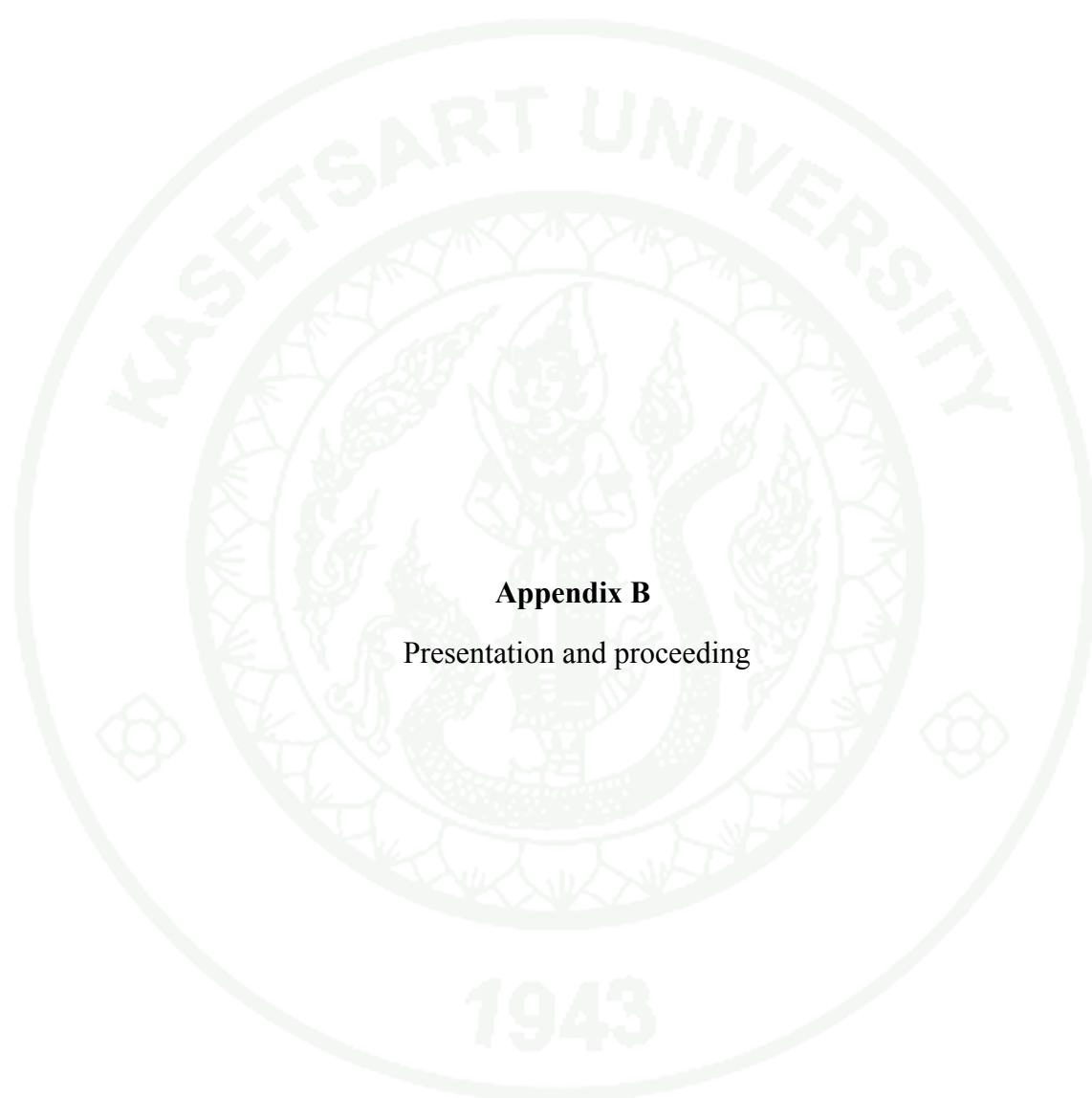
Appendix B

Presentation and proceeding

Proceedings

1. Panida Maneekobkulwong, Supa Hannongbua, Surachai Thachepan, and Songwut Suramitr. **Highly Fluorescent N,N-Dimethylaniline Derivatives: Synthesis, Photophysical and Computational Studies.** The 3rd Research Symposium on Petrochemical and Materials Technology and The 18th PPC Symposium on Petroleum, Petrochemicals, and Polymers , Ballroom, Queen Sirikit National Convention Center, Bangkok, Thailand, April 24, 2012.

CIRRICULUM VITAE

NAME   : Ms. Panida Maneekobkulwong

BIRTH DATE   : March 31, 1988

BIRTH PLACE : Chumphon, Thailand

EDUCATION :	**YEAR**	**INSTITUTE**	**DEGREE/DIPLOMA**
	2010	Kasetsart Univ.	B.Sc. (Chemistry)

POSITION/TITLE   : Postgraduated student

WORKPLACE   : Faculty of Science, Kasetsart University

SCHOLARSHIP/AWARDS :

- Kasetsart University Research and Development Institute (KURDI)
- Laboratory of Computational and Applied Chemistry (LCAC)
- The National Research University Project of Thailand (NRU)